A NEW RESPIRATORY DISEASES DETECTION MODEL IN CHEST X-RAY IMAGES USING CNN

2023
MASTER THESIS
COMPUTER ENGINEERING

Ahmed Abdulateef ALZABAQ

Thesis Advisor
Assist. Prof. Dr. İsa AVCI

A NEW RESPIRATORY DISEASES DETECTION MODEL IN CHEST X-RAY IMAGES USING CNN

Ahmed Abdulateef ALZABAQ

Thesis Advisor
Assist. Prof. Dr. İsa AVCI

T.C.
Karabuk University
Institute of Graduate Programs
Department of Computer Engineering
Prepared as
Master Thesis

KARABUK
February 2023

I certify that in my opinion the thesis submitted by Ahmed Abdulateef ALZABAQ titled “A NEW RESPIRATORY DISEASES DETECTION MODEL IN CHEST X-RAY IMAGES USING CNN ” is fully adequate in scope and quality as a thesis for the degree of Master of Science.

Assist. Prof. Dr. İsa AVCI ....

Thesis Advisor, Department of Computer Engineering

This thesis is accepted by the examining committee with a unanimous vote in the Department of Computer Engineering as a Master of Science thesis. February 16, 2023

Examining Committee Members (Institutions)	Signature
Chairman: Assist. Prof. Dr. Murat KOCA (YYU)	....
Member: Assist. Prof. Dr. Omar DAKKAK (KBU)	....
Member: Assist. Prof. Dr. İsa AVCI (KBU)	....

The degree of Master of Science by the thesis submitted is approved by the Administrative Board of the Institute of Graduate Programs, Karabuk University.

Prof. Dr. Müslüm KUZU ....

Director of the Institute of Graduate Programs

"I declare that all the information within this thesis has been gathered and presented in accordance with academic regulations and ethical principles and I have according to the requirements of these regulations and principles cited all those which do not originate in this work as well."

Ahmed Abdulateef ALZABAQ

ABSTRACT

M. Sc. Thesis

A NEW RESPIRATORY DISEASES DETECTION MODEL IN CHEST X-RAY IMAGES USING CNN

Ahmed Abdulateef ALZABAQ

Karabuk University
Institute of Graduate Programs
The Department of Computer Engineering

Thesis Advisor:
Assist. Prof. Dr. İsa AVCI
February 2023, 87 pages

Respiratory disease has a massive global health impact. Respiratory diseases, sometimes known as lung diseases, affect the lungs' airways and other components. Respiratory disease remains among the world's major causes of mortality without a doubt. To increase long-term survival rates and improve recovery possibilities, early identification is crucial. Recently, deep learning has demonstrated excellent potential for identifying diseases in medical imaging, particularly respiratory disease. Recent advances in machine learning, such as Deep Learning (DL), make it possible to identify, quantify, and categorize characteristics in medical pictures. The proposed system includes many steps in which images are treated in a variety of ways utilizing grayscale image transformation and histogram equalization. The characteristics are then reduced using a variety of approaches, including Linear Discriminant Analysis

(LDA) and Gray Level Co-occurrence Matrix (GLCM). The proposed Convolutional Neural Network (CNN) is then utilized as the system's final stage to distinguish between patients with (COVID-19, Viral Pneumonia, or Lung Opacity) and healthy people, and the system is assessed using a set of assessment criteria. Experiments have been carried out on the Covid-19 Radiography dataset by using the suggested CNN model. This dataset contains 21,165 .png images (consisting of 3616 COVID-19 positive images, 10,192 normal images, 1345 viral pneumonia images, and 6012 Lung Opacity). The dataset is split into two parts utilizing the random sampling approach, the first of which is 70% employed to train the suggested convolution neural network, while the remaining 30% is utilized to test the system later. The obtained outcomes indicate that the suggested system has given an ideal detection accuracy rate of 99.94%, and this is due to the use of feature reduction methods and the proposed convolutional neural network structure.

Key Words : Respiratory disease**,** Deep learning, Classification techniques, Convolution Neural Network (CNN), COVID-19, Chest X-ray.

Science Code : 92432

ÖZET

Yüksek Lisans Tezi

CNN KULLANARAK GÖĞÜS RÖNTGEN GÖRÜNTÜLERİNDE YENİ BİR SOLUNUM HASTALIĞI TESPİT MODELİ

Ahmed Abdulateef ALZABAQ

Karabük Üniversitesi
Lisansüstü Eğitim Enstitüsü
Bilgisayar Mühendisliği Anabilim Dalı

Tez Danışmanı:
Dr. Öğr. Üyesi İsa AVCI
Şubat 2023, 87 sayfa

Solunum yolu hastalığının küresel sağlığa büyük etkisi vardır. Solunum yolu hastalıkları akciğerlerin hava yollarını ve diğer bileşenlerini etkilediğinden dolayı bazen akciğer hastalıkları olarak da bilinir. Solunum yolu hastalıkları dünyanın önde gelen ölümcül hastalıkları arasında yer aldığı inkâr edilemez. Erken teşhis, iyileşme şansını artırmada ve uzun vadeli hayatta kalma oranını artırmada önemli bir etkendir. Derin Öğrenme son zamanlarda tıp yönünden hastalıkları tespit etmede, özellikle de solunum yolu hastalıklarını tespit etme konusunda büyük umut vaat ediyor. Derin Öğrenme (DL) ve diğer mevcut Makine Öğrenimi gelişmeleri, tıbbi görüntülerdeki özelliklerin keşfedilmesine, ölçülmesine ve sınıflandırılmasına olanak tanımaktadır. Önerilen sistem, görüntülerin gri tonlamalı görüntüye dönüşmesi ve histogram eşitleme kullanılarak birçok farklı şekillerde işlendiği çeşitli adımlar içermektedir. Karakteristikler daha sonra Doğrusal Ayırma Analizi (LDA) ve Gri Düzey Birlikte Oluşum Matrisi (GLCM) dahil olmak üzere çeşitli yaklaşımlar kullanılarak eksiltilir. Önerilen Konvolüsyonel Sinir Ağı (CNN), daha sonra (COVID-19, Viral Pnömoni ve ya Akciğer Opaklığı) hastaları ve sağlıklı insanları ayırt etmek için sistemin son aşaması olarak kullanıldı ve sistem bir dizi değerlendirme kriteri kullanılarak değerlendirildi. Önerilen CNN modeli kullanılarak Covid-19 Radyografi veri seti üzerinde deneyler yapılmıştır. Bu veri kümesi 21.165 .png görüntüsü içerir (3616 COVID-19 pozitif görüntü, 10.192 normal görüntü, 1345 viral pnömoni görüntüsü ve 6012 Akciğer Opaklığından oluşur). Veri seti, rastgele örnekleme yaklaşımı kullanılarak iki kısma bölünmüştür; bunlardan ilki, önerilen evrişim sinir ağını eğitmek için kullanılan %70, geri kalan %30 ise sistemi daha sonra test etmek için kullanıldı. Elde edilen sonuçlar, önerilen modelde öznitelik azaltma yöntemleri ve önerilen evrişimli sinir ağı yapısı kullanılmasından dolayı sistemin %99,94 gibi ideal bir tespit doğruluk oranı elde edilmiştir.

Anahtar Kelimeler **:** Solunum yolu hastalığı, Derin öğrenme, Sınıflandırma teknikleri, Konvolüsyon Sinir Ağı (CNN), COVID-19, Göğüs Röntgeni.

Bilim Kodu **:** 92432

ACKNOWLEDGMENT

I owe to my dear parents, I first and foremost give thanks to Allah the Almighty for this success and facilitation. My wonderful father gave me the most precious and priceless things to make me a man of honor. My lovely mother, who is skilled at engineering my heart with her prayers. To my family, in which I grew up, and its extension, which brings me pride and dignity. I owe a special appreciation to my thesis supervisor, Assist. Prof. Dr. İsa AVCI, who spared no effort in providing infinite assistance and direction till this thesis was completed to the best of my ability.

I also extend my thanks and gratitude to the University of Karabuk, including the wonderful professors, doctors, and colleagues who accompanied us throughout our academic journey.

I dedicate my thesis with gratitude to our motherland Iraq and the wonderful Turkey, which welcomed our scientific experiment and assisted in providing every possibility to graduate in this magnificent manner.

CONTENTS

Page

Page

Page

LIST OF FIGURES

Page

Page

LIST OF TABLES

Page

ABBREVIATIONS

1D	1 Dimensional
2D	2 Dimensional
AI	Artificial Intelligent
CNN	Convolution Neural Network
CT	Computed Tomography
CXR	Chest X-Ray
DBM	Deep Boltzmann Machine
DBN	Deep Belief Network
DeTraC	Decompose, Transfer, And Compose
DL	Deep Learning
EL	Ensemble Learning
GLCM	Gray Level Co-Occurrence Matrix
HRCT	High-Resolution Computed Tomography
LDA	Linear Discriminant Analysis
ML	Machine Learning
RNN	Recurrent Neural Networks
WHO	World Health Organization

PART1

INTRODUCTION

Respiratory diseases sometimes referred to as lung diseases, affect the lungs' airways and other structures of the lungs. It is evident that respiratory conditions rank among the world's top killers and disablers. An important factor in boosting chances of recovery and raising long-term survival rates is early identification. Skin tests, blood tests, sputum sample testing, chest X-ray examinations, and computed tomography (CT) scan examinations have historically been used to diagnose respiratory infections. Deep learning has recently demonstrated excellent potential for illness diagnosis in medical images, particularly respiratory disease[1].

A subset of machine learning called "deep learning" works with algorithms that are inspired by the structure and function of the human brain. The identification, measurement, and categorization of patterns in medical images are made possible by Deep Learning (DL) and other recent developments in machine learning. These advancements were made feasible by deep learning's capacity to discover features solely from data rather than manually designing features depending on domain-specific knowledge [2]. Deep learning is swiftly advancing to the state of the art, improving performance across a wide range of medical applications. As a result, these developments help clinicians identify and classify particular disease disorders effectively [3]. Numerous respiratory diseases, including pulmonary nodule diseases, pulmonary embolism, pneumonia, lung opacity, interstitial lung disease, pneumonia, tuberculosis, and coronavirus disease (COVID-19), have been the focus of major applications of deep learning techniques in past years [4]. About 334 million people worldwide have asthma, 1.4 million people die from tuberculosis, 1.6 million from lung cancer, and millions more die from pneumonia each year, according to the forum

Of International Respiratory Societies. Millions of individuals were affected by the COVID-19 epidemic, which put a strain on the global healthcare system [5]. The taxonomy for recent DL respiratory disease diagnosis is shown in (Figure 1.1) [6].

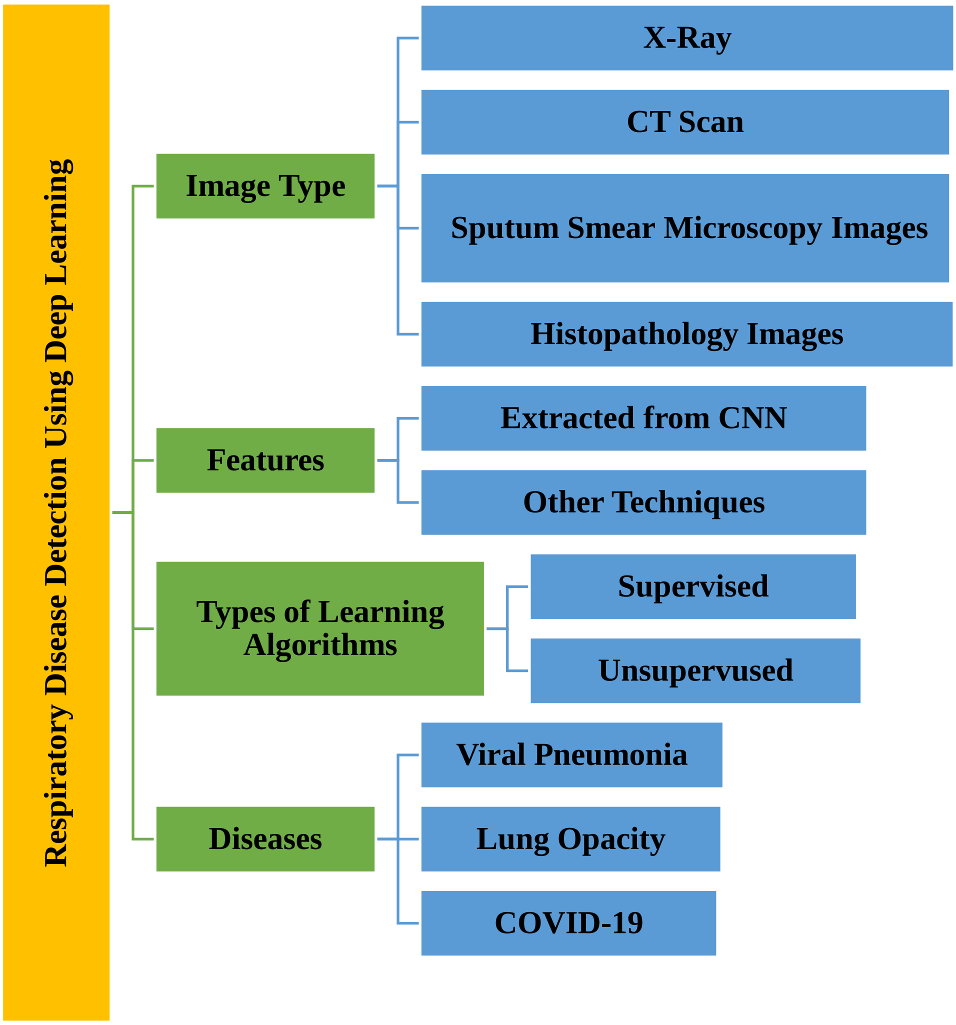

Figure 1. 1. Taxonomy of respiratory disease detection using deep learning [6].

1.1. RESPIRATORY DISEASE

In this section, three respiratory diseases: viral pneumonia, lung opacity, and COVID-19 are discussed in greater detail in Sections 1.2.1–1.2.3, respectively. These three diseases were considered as they are the most common causes of critical illness and death worldwide related to respiratory, while COVID-19 is an ongoing pandemic.

1.1.1. Viral Pneumonia Disease

Pneumonia is an infection that affects the air sacs in the lungs of the affected individual. It is caused by bacteria, fungus, or viruses invading the air sacs of the lungs, which fill up with released fluids and produce chills, fever, mucus coughing, and breathing difficulties in patients who have this ailment. Children under the age of 5, as well as older individuals with weakened immune systems, are particularly prone to these infections [7]. Pneumonia killed over a million children worldwide in 2018 and remains a potentially fatal disease if not discovered and treated early. Radiography, CT scan, or MRI are the most often used methods for identifying pneumonia. The patient's chest radiograph is examined by medical personnel to determine whether or not they have pneumonia. Furthermore, the patient’s medical history and test results are typically used to diagnose pneumonia [8].

X-rays penetrate a radiograph of the chest, where soft tissues produce a dark color, and hard tissues, including bones, provide a dazzling hue. Fluids entering the sacs called of the lungs in the chest cavity cause the radiological picture to seem brighter in patients with pneumonia. A stronger hue may suggest cancer cells, blood vessel enlargement, or a cardiac anomaly, among other things, on the lung cavities [9]. Chest x-rays are the most effective way for determining the extent and location of an infected region of the lungs. The onset of the disease might be inaccurate and misconstrued using these methods. As a result, the endeavor is rewarding in terms of improving the processing in medical circumstances in isolated areas for pneumonia detection [10].

1.1.2. Lung Opacity Disease

The Fleischner society defines lung opacity as the presence of High-Resolution Computed Tomography (HRCT) of a hazy increase in lung density that is not linked with obscuration of the underlying arteries or bronchial walls [11]. Lung opacity is a symptom of several lung diseases, including alveolar collapse, interstitial thickening, and air-space disease. It is brought on by the filling of alveolar gaps (by cells or fluid) or the thickening of alveolar walls or the interstitium. Since HRCT is primarily used for the differential diagnosis of lung opacity, lung opacity might be challenging to detect radiographically, especially in mild instances. The clinical-radiological assessment required to arrive at a reliable diagnostic hypothesis has replaced the conventional notion of lung opacity as an unspecific symptom. Finding the salient features of the actual underlying illness (such as the beginning of symptoms, smoking history, presence or absence of fibrosis, or distribution in the lung parenchyma) is a superior method [12].

1.1.3. COVID-19 Disease

In less than two years, COVID-19, commonly recognized as the worst virus of the 21st century, has killed millions of people throughout the world. Chest X-ray imaging is helpful for a precise diagnosis because the infection initially affects the patient's lungs. Rapid identification and lowering exposure to the virus among medical or healthcare professionals would benefit from any automatic, dependable, and accurate screening procedure for COVID-19 infection [13]. The COVID-19 outbreak has become one of the most serious public health problems in recent memory. The virus spreads quickly; during the early months of the pandemic, COVID-19's reproduction number ranged from 2.24 to 3.58, meaning that each infected person on average disseminated the illness to two or more people. As a result, from a few hundred cases (mostly in China) in January 2020 to more than 43 million cases globally distributed in November 2020, the number of COVID-19 infections increased [14].

The COVID-19 outbreak has become one of the most serious public health problems in recent memory. The virus spreads quickly; during the early months of the pandemic, COVID-19's reproduction number ranged from 2.24 to 3.58, meaning that each infected person on average disseminated the illness to two or more people. As a result, the number of COVID-19 infections surged from a few hundred cases (mainly in China) in January 2020 to more than 43 million cases globally in November 2020 [15]. It is believed that the coronaviruses that cause COVID-19, SARS-COV2, and MERS are related (MERS). After an average of 5.2 days of incubation, a wide range of symptoms linked to COVID-19 begin to appear. Common symptoms include a fever, a dry cough, and exhaustion. Other symptoms include headache, hemoptysis, diarrhea, dyspnea, and lymphopenia. SARS-COV-2, which first infected a human in December

2019, is primarily spread through droplets made when infected people talk, cough, or sneeze. The droplets can only spread through direct touch since they are too heavy to travel very far [16].

1.2. DEEP LEARNING FOR RESPIRATORY DISEASE DETECTION

Respiratory disease detection mainly entails classifying an image as healthy or disease-infected. Training is used to create the respiratory disease classifier, often known as a model. The process through which a neural network learns to recognize a class of images is known as training. Deep learning can be used to train a model that can identify images based on their class labels [17]. To use deep learning for respiratory disease diagnosis, the first step is to collect photos of lungs with the disease to be identified. The second phase is to train the neural network until it can recognize diseases. The final stage is to classify new images. In this case, the model is shown new images that it has never seen before, and the model guesses the class of those images. Figure (1.2) depicts various deep-learning approaches for respiratory disease detection [18].

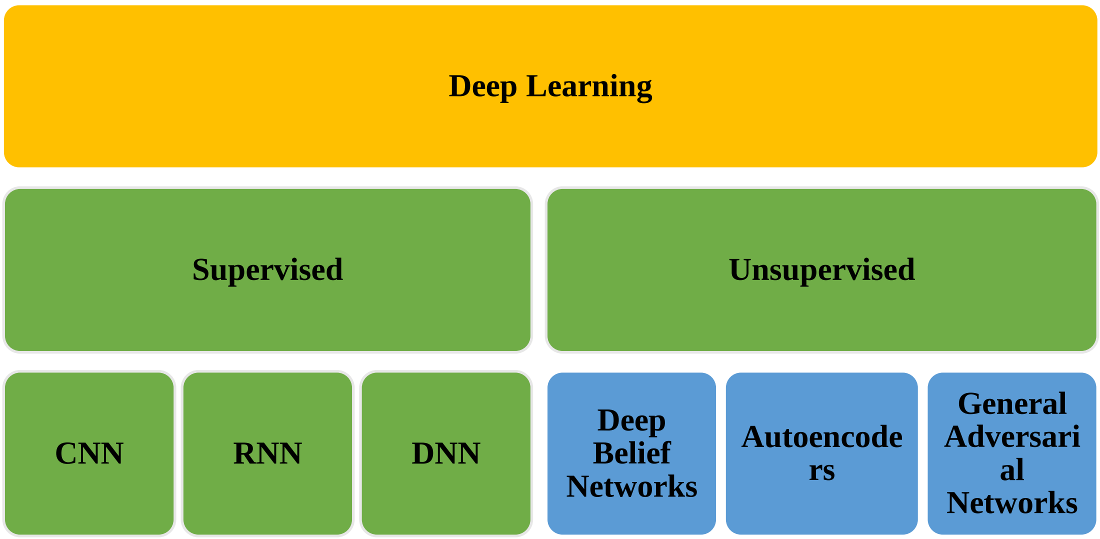

Figure 1. 2. Respiratory disease detection methods based on DL [18].

The most extensively used deep learning method is the Convolution Neural Network (CNN), which is particularly good at finding patterns in photos. CNNs, like human neural networks, are made up of neurons that may be trained in terms of biases and weights. Each neuron gets a wide range of inputs. The inputs' weighted sum is then computed. The weighted sum is then sent to an activation function, which generates an output. CNN is distinguished from other neural networks by the presence of convolution layers. Fig. (1.3) depicts a CNN architecture.

A CNN is made up of several layers, the four basic types of which are convolutional layers, pooling layers, and fully-connected layers. A "convolution" approach is used by the convolutional layer. Convolution is a linear method that multiplies the input by a collection of weights. A set of weights makes up a kernel or filter. The given data exceeds the filter's capability. A segment of the input that is the size of the filter is multiplied by the filter, producing a dot product. The dot products are then combined to produce a single value. The pooling layer gradually lowers the dimension of the feature of the representation, decreasing the number of parameters and computations in the network and, as a result, controlling overfitting. A rectified linear unit (ReLU) is added to the CNN to apply an elementwise activation function, including such a sigmoid, to the activation output of the previous layer [19].

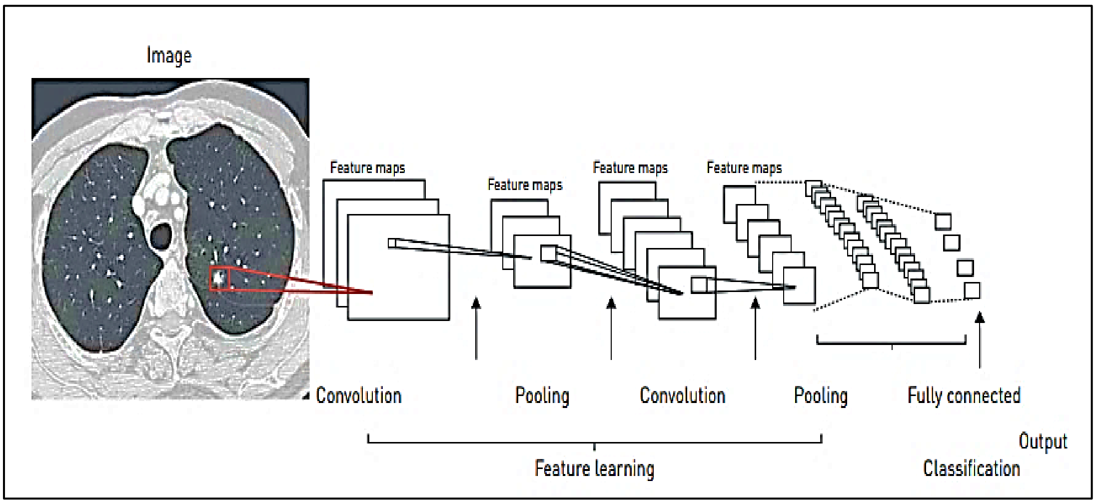

Figure 1.3. An example of a convolutional neural network (CNN) [19].

CNN normally consists of two parts throughout the learning process: feature extraction and classification. During the feature extraction step, convolution is performed to the input data using a filter or kernel. Next, a feature map is produced. During the classification step, CNN calculates the probability that the picture belongs to a certain class or label. CNN is very useful for classifying and recognizing images since it automatically learns features without the need for human feature extraction. CNN may be retrained and used in a different area thanks to transfer learning. Transfer learning has been shown to result in better classification outcomes [20].

1.3. IMAGE TYPE USED FOR RESPIRATORY DISEASE DETECTION

In the literature, chest X-rays, CT scans, sputum smear microscopy images, and histopathology images were all used to train the deep learning model. These graphics are fully explained in Sections 1.4.1-1.4.4. Positron Emission Tomography (PET) and Magnetic Resonance Imaging (MRI) are two other imaging techniques. Potential applications for PET and MRI scans include identifying medical conditions and evaluating the success of existing therapies.

1.3.1. Chest X-rays

A diagnostic exam called an X-ray helps doctors find and treat medical problems. The most common medical X-ray method produces pictures of the blood vessels, lungs, airways, heart, spine, and chest bones during a chest X-ray. Medical X-ray pictures have traditionally been revealed to photographic films, which must be processed before they can be examined. Digital X-rays are utilized to solve this problem. Figure 1.4 displays many instances of chest X-rays with diverse respiratory diseases from distinct datasets [21].

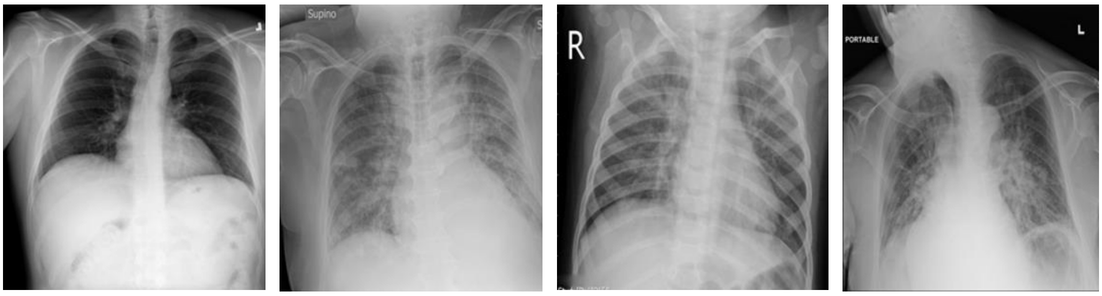

(a) (b) (c) (d)

Figure 1. 4. X-rays for lung (a) Normal (b) COVID (c) Viral Pneumonia (d) Lung Opacity [21]

1.3.2. CT Scans

A CT scan is a form of radiography that makes use of computer processing to create sectional images at various depths from images taken from various angles all over the patient's body. To generate a 3D representation of the patient that shows the tissues, organs, skeleton, and any abnormalities, the picture slices can be shown separately or stacked. Compared to X-rays, CT scan pictures offer more information. Examples of CT scan images from different datasets are shown in Figure 1.5. CT scans have been utilized to diagnose respiratory diseases in a variety of studies, including viral pneumonia diagnosis, lung opacity detection, and COVID-19 identification [22].

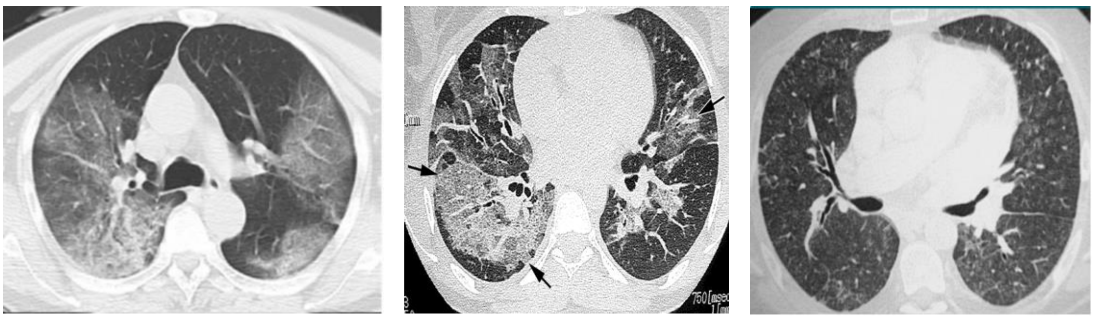

(a) (b) (c)

Figure 1. 5. CT scan for lung (a) COVID (b) Viral Pneumonia (c) Lung Opacity [22]

1.3.3. Sputum Smear Microscopy Images

Sputum is a viscous fluid that collects in the lungs and the airways leading to the lungs. To do a sputum smear examination, a very thin covering of the sputum sample is deposited on a glass slide. Figure 1.6 depicts sputum smear microscopy images [23].

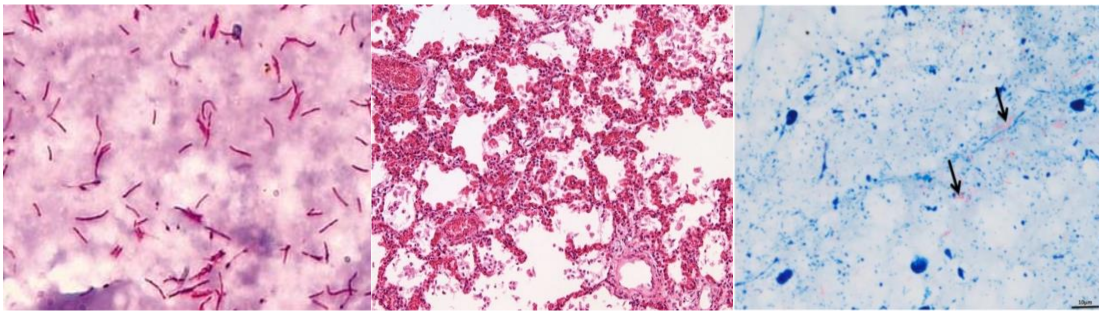

(a) (b) (c)

Figure 1. 6. Sputum smear microscopy (a) COVID (b) Viral Pneumonia (c) Lung Opacity [23]

1.3.4. Histopathology Images

Histopathology is the study of disease symptoms utilizing glass slides for microscopic evaluation of a biopsy or surgical tissue. The slices are stained with one or more dyes to help see the various tissue components. Gross and histological features of the lungs in patients with severe acute respiratory syndrome are shown in Figure 1.7 [24].

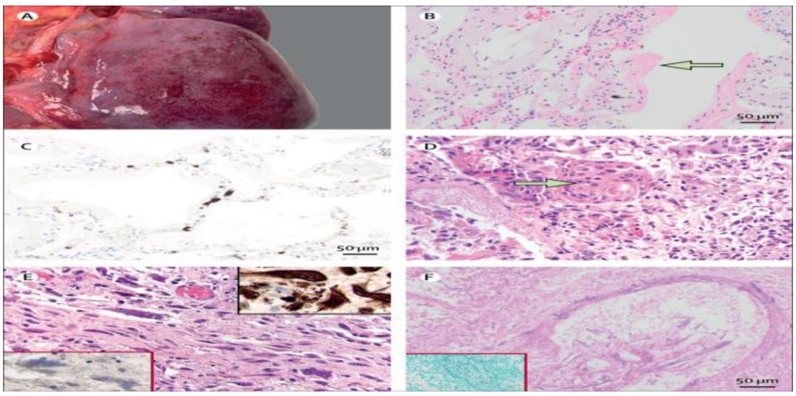

Figure 1. 7. Gross and histological features of lungs [24].

1.4. PROBLEM STATEMENT

According to the most recent WHO (World Health Organization) study, the respiratory disease affects millions of individuals worldwide, and there are 6,669,519 a death in the whole world caused by the Corona pandemic, since its appearance two years ago, until today. Perhaps some of these cases are fatal owing to a shortage of medical personnel or a human error. Manual x-ray image analysis is a time-consuming technique that requires radiological skill and a substantial amount of time. Deep learning may help in making better decisions, recognizing disease markers, doing initial examinations, and recommending urgent cases. Previous methodologies needed a vast amount of data as well as powerful processing capacity. Rather than building new algorithms to tackle an issue, we opted to harness current tools and demonstrate their high accuracy in medical tasks outperforming available alternatives.

1.5. OBJECTIVES OF THESIS

The goal of this thesis is to use CNN architecture to develop a deep learning model for respiratory disease detection and classification with high accuracy and low error rate. One of the most significant requirements in achieving this goal is classification accuracy. A quick algorithm with low accuracy is unsuitable for clinical application since missing true positives would be extremely detrimental to patients. Computer-aided image analysis algorithms now compete with professionals in terms of accuracy while remaining unrivaled in terms of speed and number of evaluated cases, thanks to recent technological breakthroughs. Unlike physicians, computers make swift, reasonable choices that are unaffected by emotions or fatigue.

1.6. CONTRIBUTION OF THESIS

This research brings a new outlook on pre-trained deep neural networks. It makes the following theoretical and practical contributions:

1. The influence of transfer learning-based classifiers trained on small Chest X-Ray data sets on accuracy.

2. Application of different feature extraction techniques to eliminate features that do not affect lung disease problem detection.
3. The efficacy of transfer learning in deep neural networks trained on a limited medical dataset.
4. Classification of more than one disease of the respiratory utilizing a proposed convolutional neural network model after a set of preprocessing.

1.7. OUTLINE OF THESIS

Aside from the current chapter, there are five chapters in this thesis, which are organized as follows:

- **Chapter Two, "Related Work":** explains the works related to the topic of the thesis.
- **Chapter Three, "Theoretical Background":** deals with the fundamental of the deep learning system, types of respiratory diseases, image processing, features extraction techniques, and the basic metrics of the detection accuracy.
- **Chapter Four, "The Proposed System":** is concerned with describing the design of the presented system.
- **Chapter Five, "Experimental Results and Discussion":** The experimental results of each of the measures in this study are shown by the reasons.
- **Chapter Six, "Conclusions and Recommendations":** This chapter presents conclusions from the research carried out and offers a collection of points for possible directions for future works.

PART 2

LITERATURE REVIEW

Deep learning has demonstrated remarkable strength in the field of medical imaging, such as disease detection and classification, as an emerging technology. Researchers are working hard to implement deep learning to detect diseases from x-rays of the chest, focusing on various aspects. The presence of unnecessary objects in the chest x-ray, as well as the reduced size due to the preprocessing process, are major challenges in the automatic detection of multiple diseases from a chest x-ray. To address these issues, a segmentation-based deep fusion network that provides detailed information about the lung region was developed [25].

Many recent studies in the medical field, particularly in medical image processing techniques, have been conducted by many researchers. They used techniques such as Machine Learning (ML) and Deep Learning (DL), among others. Machine learning (ML) technologies are widely acknowledged as important tools for improving disease prediction and diagnosis. To create better ML models, however, efficient extraction methods are required. Deep learning models are often employed in medical imaging systems because they can dynamically extract the features or use pre-trained networks.

In 2020, S. Asif et al. [26]. attempted to automatically recognize COVID-19 pneumonia patients using digital chest x-ray images while optimizing detection accuracy with deep Convolutional Neural Networks (CNN). There are 864 COVID-19 images in the collection, 1345 viral pneumonia images, and 1341 normal chest x-ray images. This study proposed the CNN-based model Inception V3 with transfer learning for detecting coronavirus pneumonia-infected patients using chest X-ray radiographs, and it achieves a classification accuracy of more than 98%.

M. Hussain and Y. Shiren [27]. used chest X-rays to test Convolutional Neural Networks (CNNs) for COVID-19 classification. CNN performance with one, three, and four convolution layers is assessed. The collection consists of 13,808 CXR images. The first experimental findings suggest that the CNN model with three convolution layers can consistently identify 96% accuracy on X-ray images with three divisions of the dataset. This demonstrates the potential of the proposed methodology for accurate COVID-19 screening.

Y. Tang et al. [28]. created and tested several deep Convolutional Neural Networks (CNNs) for distinguishing between normal and pathological frontal chest radiographs to warn radiologists and clinicians of probable problematic findings for task list triaging and reporting prioritizing. A CNN-based model classified normal vs abnormal chest radiographs with an accuracy of 94.64 ± 0.45%. For normal versus abnormal lung opacity classification, the CNN model achieved an accuracy of 94.71 ± 0.32%. Pre-training using natural images is beneficial for a moderate-sized training image set of around 8500 images. The exceptional diagnostic accuracy found in this study demonstrates that deep CNNs may reliably and effectively discern between normal and abnormal chest radiographs, thereby benefiting radiology workflow and patient care.

M. Pandit et al. [29]. suggested a model for assessing whether a subject is infected or not utilizing chest radiographs, which are one of the most extensively utilized imaging tools for clinical diagnosis due to their speed and low cost. This study comprised 1428 chest radiographs of COVID-19-positive positive participants with common bacterial pneumonia and healthy subjects (no infection). They examined the pre-trained VGG-16 algorithm for classification tasks in this work. Transfer learning with fine-tuning was used in this study to efficiently train the network using relatively small chest radiographs. Initial experiments demonstrated that the model gave good results and that it can be used to significantly accelerate COVID-19 identification. In two and three outcome class scenarios, respectively, the trial provided 96% and 92.5% accuracy. This study might be used as an initial screening, enabling healthcare providers to continue treating COVID-19 patients by detecting and screening for the disease early. In 2021, S. Jadon et al. [30]. COVID-19 was detected using well-known data scarcity techniques in deep learning. These include data augmentation, transfer learning, few-shot learning, and unsupervised learning. They also proposed a custom few-shot learning strategy based on Siamese networks for detecting COVID-19. Their experimental results showed that by employing few-shot learning methodologies, they were able to develop an efficient and accurate deep-learning method for COVID-19 identification with less data. The proposed strategy achieves 96.4% accuracy, up from 83% using baseline models.

A. Uddin et al. [31]. presented an evaluation of a Convolutional Neural Network (CNN) to detect COVID-19 from chest X-ray (CXR) images, which makes the test faster and more reliable. Because there have been several studies on this subject, the created model focuses on enhancing accuracy and employs a transfer learning approach as well as a proprietary model. Deep feature extraction has been accomplished using pre-trained deep CNN models such as VGG16, InceptionV3, MobileNetV2, and ResNet50. The classification accuracy was used to measure performance in this study. According to the findings of this study, deep learning can distinguish SARS-CoV-2 from CXR images. The developed model had 93% accuracy and 98% validation accuracy, while per-trained customized models like MobileNetV2 had 97% accuracy, InceptionV3 had 98% accuracy, and VGG16 had 98% accuracy. InceptionV3 has the highest accuracy among these models.

P. Mahesh et al. [32]. developed and presented research on how Convolutional Neural Networks (CNNs) perform exceptionally well in the identification of COVID images. Despite the requirement for a large number of images, CNNs have the potential to diagnose respiratory disorders with the highest accuracy, with an accuracy of 95% train accuracy and 98% validation accuracy.

D. Yang et al. [33]. utilized transfer learning techniques to overcome the lack of data and shorten the training time. The modified VGG16 deep transfer learning architecture was used to classify X-ray images into binary and multi-class categories. Enhanced VGG16 detected X-ray images from COVID-19 and pneumonia with 99% accuracy. The accuracy and validity of the algorithms were assessed using well-known public datasets from X-ray and CT-scan.

D. Arias-Garzón et al. [34]. used deep learning models which processed and classified images as positive or negative for COVID-19 (VGG19 and U-Net). The proposed system consists of a lung segmentation stage for preprocessing, which eliminates background elements that are irrelevant to the task at hand and could lead to biased results; a classification model trained using a transfer learning scheme; and finally, results analysis and interpretation via heat maps visualization. The most accurate models found COVID-19 with a 97% accuracy rate.

In 2022, M. Hossain et al. [35]. presented a fine-tuned ResNet50 model that correctly classified COVID-19 from chest X-ray pictures using transfer learning. For this purpose, they updated the ResNet50 scheme by adding 2 more fully linked layers to the baseline ResNet50 model. They used 10 different pre-trained weights that were trained on a variety of large-scale datasets utilizing different techniques like supervised learning and self-supervised learning. In the two-class classification, the suggested work obtained 99.17% validation accuracy and 99.95% train accuracy for COVID cases (COVID and Normal).

W. Boulila et al. [36]. intended to increase the utility of chest X-ray pictures while protecting the privacy of the data contained in them The method proposed consists of two steps: encrypting the dataset with partially homomorphic encryption and training/testing the DL algorithm on the encrypted photos. In experiments using the COVID-19 Radiography dataset, the MobileNetV2 model achieves an accuracy of 94.2% over plain data and 93.3% over encrypted data.

S. Gafoor et al. [37]. Deep Learning Multi-layered networks were used to classify the chest images as positive or negative for COVID. The proposed model is based on a dataset of Coronavirus-infected people whose chest X-rays revealed multilobar involvement. The study examined 6500 photos in total. The Convolutional Neural Network (CNN) model was trained, and it achieved a validation accuracy of 94%.

S. Asif et al. [38]. presented a robust deep learning strategy with high accuracy and a low false negative rate for identifying COVID-19 patients from chest X-rays. The proposed method is a lightweight shallow CNN with optimal parameters for detecting

COVID-19 instances in chest X-ray images. The researchers used open-source chest X-rays from healthy people and COVID-19 patients for the study. Their model achieves 99.68% accuracy in the classification of healthy and COVID-19-infected individuals.

R. Sarki et al. [39]. presented a deep learning-focused technique for classifying and detecting COVID-19 instances in x-ray images. Their model is fully automated, capable of categorizing binary classes with 100% accuracy using VGG16 and multi-class classes with 93.75% accuracy using a constructed CNN.

M. Hashmi et al. [40]. suggested a model trained on digital chest X-ray images that is effective for detecting pneumonia. This model could help radiologists make decisions. Weighted predictions from cutting-edge deep learning models such as ResNet18, Xception, InceptionV3, DenseNet121, and MobileNetV3 are optimally combined using a revolutionary weighted classifier method. This method is a type of supervised learning in which the network forecasts the outcome based on the training dataset’s quality. Transfer learning is used to tune the deep learning models, resulting in an accuracy of 98.43%.

M. Karar et al. [41]. suggested a deep learning framework with two significant enhancements. To begin, a set of binary classifiers was used to automate the difficult multi-label classification of X-ray images for each tested case of health condition. That simulates a clinical setting to diagnose potential ailments for a patient. Second, the cascaded architecture of the COVID-19 and pneumonia classifiers enables the flexible deployment of multiple finely calibrated deep-learning models at the same time, resulting in the best performance in terms of confirming infected patients. In this work, eleven pre-trained convolutional neural network techniques are used. The proposed classifiers had the highest detection accuracy of 99.9%. L. Brunese et al. [42]. presented a three-step strategy, the first of which is to see if pneumonia can be seen on a chest X-ray. The second step is to distinguish between COVID-19 and pneumonia. The final phase aims to identify the X-ray regions that indicate the presence of COVID-19. The effectiveness of the suggested method was demonstrated by analyzing

6523 chest X-rays from various institutions. The average time for COVID-19 identification was 2.5 seconds, with 97% accuracy.

L. Apostolopoulos et al. [43]. The cutting-edge convolutional neural network known as Mobile Net is used and trained from scratch to examine the significance of the retrieved features for the classification job. A large dataset of 3905 X-ray images pertaining to 6 diseases is used to train MobileNet v2, which has demonstrated excellent performance in similar tasks. Among the seven classes, the classification accuracy is 87.66%.

A. Mabrouk et al. [44]. Ensemble Learning (EL) is a computer-aided classification of pneumonia that aims to simplify chest X-ray image diagnosis. Instead of building CNN models from scratch, they base their concept on existing Convolutional Neural Network (CNN) models, which have recently been utilized to improve the performance of a variety of medical tasks. The suggested model is trained using the chest X-ray data set. The proposed EL method outperforms other cutting-edge techniques currently in use, with a 93.91% accuracy.

N. Ullah et al. [45]. A brand-new CovidDetNet classification strategy was proposed to detect COVID-19 from chest radiograph images accurately and quickly. The images generated by image resizing are then fed into a CovidDetNet model designed to detect COVID-19. COVID-19 detection has an accuracy rate of 98.40%.

A. Abbas[46].Deep convolutional neural networks (CNNs) for image classification tasks have made significant progress as a result of the widespread availability of large-scale annotated picture datasets. CNN allows for the direct learning of highly representative and hierarchical local image features from data. The availability of annotated data, particularly in the medical imaging sector, remains the field's most difficult hurdle. By transferring information from generic image recognition tasks to medical image classification, transfer learning can give a promising and successful solution. Transfer learning, on the other hand, frequently fails to produce a robust solution due to anomalies in the dataset distribution. Class decomposition makes it easy to understand a dataset's class boundaries and, as a result, can cope with any anomalies in the data distribution. Motivated by this difficult task, the study offers the Decompose, Transfer, and Compose (DeTraC) technique, a unique CNN architecture based on class decomposition that uses transfer learning and class decomposition to enhance the performance of medical picture categorization. DeTraC facilitates learning at the subclass level, which is more separable and has the potential for faster convergence. Our suggested method was verified using three separate cohorts of chest X-ray pictures, histological images of human colorectal cancer, and digital mammograms. We compared DeTraC to cutting-edge CNN models to show its superior performance in terms of accuracy, sensitivity, and specificity.

S. Latif [47]. The World Health Organization (WHO) proclaimed COVID-19, an infectious illness caused by the SARS-CoV-2 virus, a pandemic in March 2020. More than 2.8 million people have tested positive at the time of writing. Infections are increasing at an alarming rate, and enormous efforts are being undertaken to combat the disease. They seek to formalize ongoing data science initiatives in this field in this publication. They evaluate public datasets and repositories that may be utilized for future work to track COVID-19 dissemination and mitigation methods, in addition to examining the fast-developing corpus of current research. They give a bibliometric study of the papers generated in this brief period as part of this. Finally, they identify common issues and traps seen throughout the examined works, elaborating on these findings. They have established a live resource repository1 that they hope to maintain up to date with the most recent materials, such as new articles and datasets. Table 2.1 presents a summary of these works.

Table 2. 1. Summary of related work.

Ref. no.	Dataset	Technique	Accuracy	No.of.class
[26]	Covid-19 Radiography	Convolutional Neural Networks (CNN)	98%	3
[27]	Covid-19 Radiography	Convolutional Neural Networks (CNN)	96%	2
[28]	Covid-19 Radiography	Convolutional Neural Networks (CNN)	94.64%	2
[29]	Covid-19 Radiography	CNN model (VGG16)	96%	3
[30]	Covid-19 Radiography	Convolutional Neural Networks (CNN)	96.4%	3
[31]	Covid-19 Radiography	CNN model (InceptionV3)	98%	2
[32]	Covid-19 Radiography	Convolutional Neural Networks (CNN)	98%	2
[33]	Covid-19 Radiography	CNN model (VGG16)	99%	3
[34]	Covid-19 Radiography	CNN models (VGG19 and U-Net)	97%	3
[35]	Covid-19 Radiography	CNN model (ResNet50)	99.17%	2
[36]	Covid-19 Radiography	CNN model (MobileNetV2)	94.2%	4
[37]	Covid-19 Radiography	Convolutional Neural Networks (CNN)	94%	2
[38]	Covid-19 Radiography	Convolutional Neural Networks (CNN)	99.68%	2
[39]	Covid-19 Radiography	CNN model (VGG16)	93.75%	3
[40]	Covid-19 Radiography	ResNet18, Xception, InceptionV3, DenseNet121, and MobileNetV3	98.43%	2
[41]	Covid-19 Radiography	Convolutional Neural Networks (CNN)	99.9%	2
[42]	Covid-19 Radiography	Convolutional Neural Networks (CNN)	97%	3
[43]	Covid-19 Radiography	Convolutional Neural Networks (CNN)	99.18%	2

[44]	Covid-19 Radiography	Convolutional Neural Networks (CNN)	93.91%	2
[45]	Covid-19 Radiography	Convolutional Neural Networks (CNN)	98.40%	3
[46]	Covid-19 Radiography	Convolutional Neural Networks (CNN)	96%	2
[47]	Covid-19 Radiography	Convolutional Neural Networks (CNN)	95.20%	3

PART 3

THEORETICAL BACKGROUND

Respiratory disease affects millions of individuals worldwide. Chronic obstructive pulmonary disease (COPD), asthma, pneumonia, lung cancer, tuberculosis, and COVID-19 are the most frequent of these diseases. Because respiratory disease spreads quickly, it is critical to detect the problem and treat the patient as soon as possible [48]. Radiologists primarily use chest X-rays to detect and diagnose respiratory illnesses. Chest X-rays can be used by radiologists to diagnose and identify diseases and a variety of other ailments [49,50]. Deep learning techniques and vast datasets enable the system to equal the performance of medical professionals in a variety of medical imaging tasks. Automatically generated diagnostic rules have improved specialist doctors' diagnostic accuracy [51,52].

3.1. OVERVIEW OF RESPIRATORY DISEASES

One of the most intriguing scientific subjects in recent years has been the study of respiratory diseases and their classification. With the numerous applications of medical pictures in hospitals, pathologies, and diagnostic centers, the quantity of medical image databases is rapidly growing to capture disorders in hospitals. Despite much research on the subject, this discipline remains perplexing and difficult to navigate. There are several ways in the literature for classifying medical images [53]. The fundamental disadvantage of previous approaches is the semantic gap between low-level visual information acquired by imaging equipment and high-level semantic information experienced by humans. The difficulties of querying and maintaining enormous datasets lead to the development of a new mechanism known as a deep convolutional neural network. Deep learning approaches have lately demonstrated excellent results in the fields of computer vision and medical engineering [51].

3.2. DIGITAL IMAGE PROCESSING

The process of converting an image signal into a digital signal and processing it with a computer is referred to as digital image processing. Image enhancement, noise reduction, segmentation, restoration, encoding, compression, and feature extraction are all part of this process. Image processing technology cannot be developed without the advancement of computers, mathematics, and the expansion of application requirements in a variety of industries. Image processing technology began to be applied more scientifically in the 1960s, and people employed it to undertake idealized processing of output images [54]

An image can be defined as a two-dimensional function, f (x, y), where x and y are spatial (plane) coordinates, and the amplitude of "f" at any pair of coordinates (x, y) is referred to as the image's intensity or gray level at that location. A digital image is one in which x, y, and the amplitude values of f are all finite, discrete quantities. The field of digital image processing refers to the processing of digital images using a computer. It is important to note that a digital image is made up of a finite number of elements, each with its location and value. Image elements, image elements, and pixels are all names for these elements. Pixel is the most commonly used term to describe the pieces of a digital image [55].

The following three tiers of image processing processes are defined in the literature[56].

1. **Low-Level image processing:** This category includes simple picture operations where both the input and the output are images, such as contrast improvement, noise reduction, etc.
2. **Mid-level image processing:** covers procedures such as the extraction of characteristics from photographs (such as edges, contours, regions, etc.).

3. **High-Level image processing:** This group of operations includes complex image processing tasks including scene analysis and interpretation for decision-making.

3.2.1. Types of Digital Images

A two-dimensional array or a two-dimensional sequence of pixels constitutes a digital image. As a result, an image is conveyed by a group of pixels that are consistently arranged in a meaningful order. Binary, grayscale, and color images are used to represent digital images [57].

1. Binary Image

It is an image that was made with the idea of having two possible standards for every pixel. Any combination of the two colors black and white, which were utilized to produce the binary artwork, can be employed. The central color, which makes up the majority of the graphic, is the color utilized for any item in the piece. Also known as "bi-level and two-level," these binary descriptions have two levels. In general, these are referred to as “black and white”, “B and W” and “monochromatic or monochrome,” however some visuals, such as grayscale descriptions, may also be ascribed to these terms.

2. Color Image

Color images can be represented by three identical 2D arrays, one for each color channel: red (R), green (G), and blue (B). Each array entry has an 8-bit value that indicates how much red, green, or blue is present at that moment on a [0, 255] scale. Three 8-bit values combined into a 24-bit integer produce 224 (16,777,216, sometimes known as 16 million or 16 M) possible color combinations. The alpha channel, a fourth channel that provides a level of transparency for each pixel and is frequently used in picture editing effects, is included in another version that uses 32 bits per pixel.

3. Grayscale Image

Every pixel value in a grayscale digital image is a component of a single sample and is easily arranged. Images in this category, which is often referred to as "black and white," are made up of gray sunglasses that change from black on the weakest side to white on the strongest side. Colorless or achromatic descriptions are known as grayscale descriptions. Each pixel's importance in a grayscale image corresponds to a certain level or capability of brightness. In physics, the words strength and brightness are used to define a light’s power density. The word "brightness" is frequently used to refer to perceived strength in optical sensitivity's psychological intelligence.

- **Image Grayscale Transformation**

Although color has a lot of potentials, the data provided by color images might take a long time to process when compared to greyscale. Color photos have inhomogeneous data, whereas greyscale images are homogeneous and can thus be handled as a single entity without the need for window adaptation. The procedure of grayscale image transformation is shown in Eq. (3.1).

$$Gray\ Image\ = (0.21\ R\ +\ 0.72\ G\ +\ 0.07\ B) \tag{3.1}$$

Since humans perceive green the most, the luminosity equation accounts for this by giving green (G) the most weight.

3.2.2. Typical Image Processing Operations

In image processing, several methods and algorithms are employed. The most typical image processing processes are as follows:

1. **Image Binarization**

A color image or a grayscale image can be converted to binary to speed up and simplify several image processing procedures. Binarization is the process of converting a color or grayscale image to a binary image with only two levels of gray (black and white). Normally, low image quality caused by noise, light, camera artifacts, and image deterioration hindered the binarization procedure. Gradient-Based Thresholding is a novel binarization approach that uses gradient-based thresholding to create a threshold surface. This approach consists of three steps: first, build the inverted image T (i, j), then determine the k value between -255 and 255, and finally, use binarization to separate the object from the context. Binarization is calculated using Eq. (3.2) as follows:

$$result\ (i.j) = \begin{Bmatrix} 0.(object) & if\ I(i.j) < T\ (i.j) + k_0 \\ 255.(background) & if\ I(i.j) > T\ (i.j) + k_0 \end{Bmatrix} \tag{3.2}$$

where I (i, j) is the intensity of the original image and k_0 is the minimum sum of absolute difference intensity[58].

2. **Image Smoothing:** a method for blending or blurring an object's characteristics in a picture. Due to the wide variety of picture smoothing techniques, a specialized smoothing technique may be developed based on the relevant mathematical model generated by the particular noise function. These are these algorithms[59].

   - **Mean filtering method:** A straightforward linear technique or method for processing spatial data is mean filtering. Its function is to provide a particular template for the defined pixels in the image, and the surrounding pixels are a component of that template. For the 33 templates, for instance, the target pixel is surrounded by eight neighboring pixels that are used to form a filter template. The original pixels are then changed to the average value of all the linked pixels in the template, in lieu of the original pixels. The neighborhood average method of mean filtering is a spatial domain processing algorithm. Consider an image f (x, y), which is an N×N array, and the processed image g (x, y). The gray level of each pixel is determined by the average gray level of multiple pixels within a predetermined neighborhood of (x, y), as described by Eq. (3.3).

$$g(x.y) = \sum f(i.j)/m\,.\,(i.j) \in s \tag{3.3}$$

Where x and y are integers from 0, 1, 2, ..., to M which is the number of pixels in the neighborhood, and S is the coordinates of each pixel in the domain.

- **Median filtering method:** In nonlinear smoothing, the median filter technique can remove image noise. Its operating technique is to replace the gray value of an image pixel with the domain gray value's median value. The following Eq. (3.4) can be used to express the two-dimensional median filter:

$$y\,(i.j) = \text{Med}\ f(i.j) \tag{3.4}$$

Where f (i, j) is a two-dimensional data sequence. The median filter's smoothing impact is primarily represented in the fact that it may not only remove noise from an image but also protect the image's edge, so improving image quality and achieving a certain restoration effect. However, there are still issues that cannot be resolved.

3. **Image Sharpening:** Sharpening techniques are image processing techniques that improve the edges and fine details of objects in an image for human viewing. Sharpen filters are one of the most commonly used and abused post-processing techniques. Sharpening, when used correctly, can improve the image by making it look crisper and more defined. However, there is a tendency to overdo it, and the image might appear artificial and "oversharpened". There is a common assumption that sharpening a fuzzy image would make it appear clearer. What happens is that the blurry image becomes even worse. The sharpening operation can be represented by Eq. (3.5) as follows [60]

$$S(i.j) = x\ (i.j) + \lambda \cdot f\ (i.j) \tag{3.5}$$

Where $x\ (i.j)$ is the original pixel value at the coordinate (i, j), $f\ (i.j)$ is the high-pass filter, λ is a tuning parameter greater than or equal to zero, and $S(i.j)$ is the sharpened pixel at the coordinate (i, j). The value taken by λ depends on the grade of sharpness desired. Increasing λ yields a sharpened image.

4. **Noise Removal and image blurring:** Before processing, noise removal filters are used to reduce the amount of noise in images. Depending on the type of noise or blur in the image, an image removal approach may be utilized. The image blurring approach can be implemented in a variety of ways, some of these types are [61]
   - **Gaussian Blur:** It is a convolution technique that is used as a preprocessing stage in many computer vision algorithms for smoothing, blurring, and removing noise from images. Gaussian blur is a linear low-pass filter that uses the Gaussian function to calculate the pixel value. The sum of two 1 Dimensional (1D) Gaussian functions is the 2 Dimensional (2D) Gaussian function, as shown in equation (3.6):

$$G(x.y) = \frac{1}{2\pi\sigma^2}\, e^{-\frac{x^2+y^2}{2\sigma^2}} \tag{3.6}$$

   - **Average Blur:** it was only one of the many techniques available for removing blur and noise from an image. When the input image has noise, this method might be employed.

5. **Edge Detection:** Edge detection is more common for detecting gray-level discontinuities than for recognizing isolated points and thin lines since isolated points and thin lines are uncommon in most practical images. The edge denotes the separation of two sections with significantly differing gray-level features. It is assumed that the transition between two zones can be properties in this case. The assumption here is that the transition between two zones can be determined solely by gray-level discontinuities. The most common edge detection techniques are [62].

- Sobel Operator
- Prewitt's Operator
- Robert's Cross Operator
- Laplacian of Gaussian
- Canny Operator

6. **Image Segmentation:** Segmentation is the process of splitting an image into several pieces. Segmentation is a pre-processing step for object recognition and classification. Many image segmentation techniques have been developed by researchers and scientists, and some of the most important and widely used image segmentation techniques are [63].

- Threshold-Based Image Segmentation.
- Region-Based Image Segmentation.
- Edge-Based Image Segmentation.
- ANN-Based Image Segmentation.

7. **Histogram Equalization**

Histogram equalization is a spatial domain contrast enhancement strategy in image processing that uses the image's histogram. Histogram equalization frequently increases the processed image's global contrast. This technique works nicely with both bright and dark images. The histogram was done by applying Eq. (3.7) as follows [64].

$$h[i]=\sum_{x=1}^{N}\sum_{y=1}^{M}\begin{Bmatrix} 0 & \text{if } f[x.y]=i \\ 1 & \text{otherwise} \end{Bmatrix} \tag{3.7}$$

the cumulative distribution is then calculated by Equations (3.8) and (3.9) as follows:

$$\mathrm{cdf}(X_i) = \sum_{i=0}^{k} p(X_i) \tag{3.8}$$

$$g[x.y] = \frac{\mathrm{CDF}\ [f[x.y] - \mathrm{CDF}_{min}]}{(N \times M) - \mathrm{CDF}_{min}} \times (L-1) \tag{3.9}$$

8. Image Resize

Image resizing technology is quickly becoming a research hotspot due to the advent of varied display device sizes in recent years, which unavoidably results in images being reduced in size or enlarged (a process known as resizing). This method considers the content of the image in addition to the geometry size limits when resizing the images because each content requires various approaches. To accomplish the goal of resizing, high degrees of key parts are kept as nearly unchanged as feasible while less important areas are modified a few sizes larger. Image retargeting is another name for the practice of image resizing. For the aim of resizing, the bilinear interpolation approach might be utilized. Due to their numerical simplicity, bilinear interpolation techniques are among the most well-known approaches employed in image processing. Linear interpolation along both axes, two linear interpolations along the x-axis, and one linear interpolation along the y-axis are the components of bilinear interpolation. Point R1 (x, y) is defined as:

$$R1(x, y) = Q11 \bullet (x2 - x) / (x2 - x1) + Q21 \bullet (x - x1) / (x2 - x1) \tag{3.10}$$

Point R2(x, y) is defined as:

$$R2(x, y) = Q12 \bullet (x2 - x) / (x2 - x1) + Q22 \bullet (x - x1) / (x2 - x1) \tag{3.11}$$

The interpolated point P (x, y) is defined as:

$$P(x, y) = R1 \bullet (y2 - y) / (y2 - y1) + R2 \bullet (y - y1) / (y2 - y1) \tag{3.12}$$

Where, Q11, Q21, Q12, and Q22 are the positions of the known closest points, x and y are the coordinates of the points, P desired point, and R point on the line with the known points [65].

3.2.3. Medical Image Analysis

Due to its significant clinical impact and ongoing challenges, medical image analysis has been a broad and active field of study in recent decades. In 1895, Wilhelm Röntgen discovered X-rays and was the first to record a two-dimensional X-ray picture of a human body component, as seen in Figure 3.1, a. This discovery marked the beginning of a new era in medical imaging, which has subsequently grown to become the most prevalent form of examination. A two-dimensional projection imaging approach in which an object is projected onto a detector is known as traditional radiography. X-rays are emitted by the X-ray tube and pass through things. Because of material densities and attenuation coefficients, the intensity of X-rays is dispersed or attenuated (i.e., bones, tissues, and fluids). Most radiography systems today employ a digital X-ray detector to transform X-ray radiation into an image. The active picture area of a typical detector is 34.48 cm ×42.12 cm, and the generated image has a matrix size of 2330×2846 pixels and a bit depth of 14 bits. Digital detectors are classified as either direct or indirect radiation converters, with the latter being more frequent. The absorbed X-rays are converted directly into electric current using a digital detector with direct conversion. The indirect conversion, on the other hand, employs a scintillator layer to transform the X-radiation into the light. The light is subsequently captured by photodiodes for final conversion into an electric current in Figure 3.1, b [66].

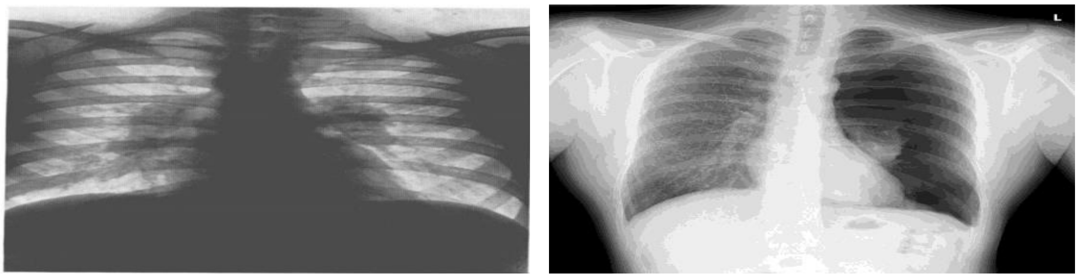

(a) **(b)**

Figure 3. 1. (a). One of the first chest X-rays and (b). Modern medical chest X-ray [66].

Twenty-one years later, the most prevalent type of examination in radiology departments is a chest X-ray. The basics of chest X-ray interpretation and diseases are covered. The way the radiation beam passes through the patient is usually used to designate chest X-rays. Radiologists often enhance their grasp of chest X-rays and diagnostic skills after mastering the fundamentals of chest X-ray analysis. Over time, radiologists learn what a healthy patient's chest X-ray looks like and compare each new patient to this memorized depiction. Figure 3.2 explain examples of chest X-ray [67].

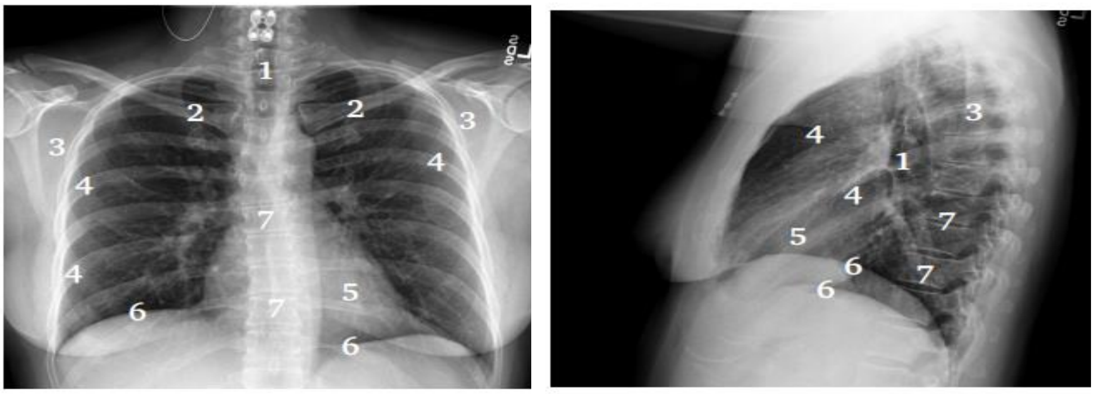

(a) **(b)**

Figure 3. 2. (a) Frontal chest X-ray and (b) Lateral chest X-ray [67].

3.3. FEATURE EXTRACTION TECHNIQUES

Features are the specific information needed to address a particular application and represent important aspects of images. The training set requirements and classification accuracy are significantly impacted by the choice of input characteristics. The procedure of extracting features from images reduces the number of resources needed by capturing the visual content of the images Some of these techniques can be listed as follows:

3.3.1. Linear Discriminant Analysis (LDA)

It is a technique for obtaining supervised linear features. However, some research indicates that LDA may be utilized as a linear classifier. To improve class separation, LDA creates a new feature space in which to build data. It generates k distinct independent features from a dataset's d independent attributes that optimally distinguish the classes (dependent features). As a result, the number of created components is less than the number of classes. LDA begins by generating two scatter matrices, as illustrated in Equations (3.13) and (3.14):

1. An in-between-class matrix (SMb) displaying the distance between each class's means.

2. A within-class matrix (SMw) determines the separation between each class's mean and the data within it. Determine the scattering matrices' Eigenvalues and corresponding Eigenvectors, then organize the Eigenvectors according to their calculated Eigenvalues.
3. Build matrix W (d×k) using k top Eigenvectors.
4. Transform X using 5 to obtain the new subspace Y = X · W

$$SMb = \sum_{k=1}^{m} N_k(\mu_k - \mu)(\mu_k - \mu)^T \tag{3.13}$$

$$SMw = \sum_{k=1}^{m} \sum_{x=1}^{n} N_k(x - \bar{\mu}_k)(\mu - \bar{\mu}_k)^T \tag{3.14}$$

where denotes the overall mean, k is the mean, and μ denotes the number of classes. Also, N_k is the size of the related classes, and "μk" is the mean vector of the class [68].

3.3.2. Gray Level Co-occurrence Matrix (GLCM)

A simple method called GLCM is utilized to extract from images the textural properties including Energy, Contrast, Correlation, and Homogeneity. When used in calculations, the histogram solely conveys data about density distribution; it contains no information about the spatial relationships between pixels. One statistical method is the use of co-occurrence matrices to extract features that indicate the distribution of intensities and relative locations of nearby pixels in an image. If image H of dimension M×M, the co-occurrence matrix C can be written as:

$$c(i.k) = \sum_{y=1}^{M} \sum_{z=1}^{M} \begin{Bmatrix} 1 & if\ H\ (y.z) = i\ and\ H(y + \Delta y.z + \Delta z) = j \\ 0 & otherwise \end{Bmatrix} \tag{3.15}$$

Where (Δy, Δz) denotes the separation between the relevant pixel and its neighbor [69].

3.4. HISTORY OF ARTIFICIAL NEURAL NETWORKS

About 86 billion biological neurons make up the large biological neural network that makes up the human brain, which functions as a complex, parallel, nonlinear computer. The cornerstone for creating an artificial neural network is the neuron, which is the fundamental signal unit of our brain structure. Its reduction into a mathematical model provides this basis. Fig. (3.3, a) depicts a biological neuron, while Fig. (3.3, b) depicts an artificial neuron. Biological neurons receive impulses via dendrite-based synapses. The input signal x_i is multiplicatively weighted based on synaptic strength w_i.

$$y = f(a) = f(\sum_{i=0}^{l} w_i x_i + b) \tag{3.16}$$

where "a" is the output of the artificial neuron before an activation function f, I is the running index divided by the total number of input signals l, and b is the bias. The foundation of artificial neural network theory is the assumption that the trainable parameters w, I, and b control how much power one artificial neuron has over other artificial neurons. From this point on, "neuron" and "neural network" will always refer to the synthetic model [70].

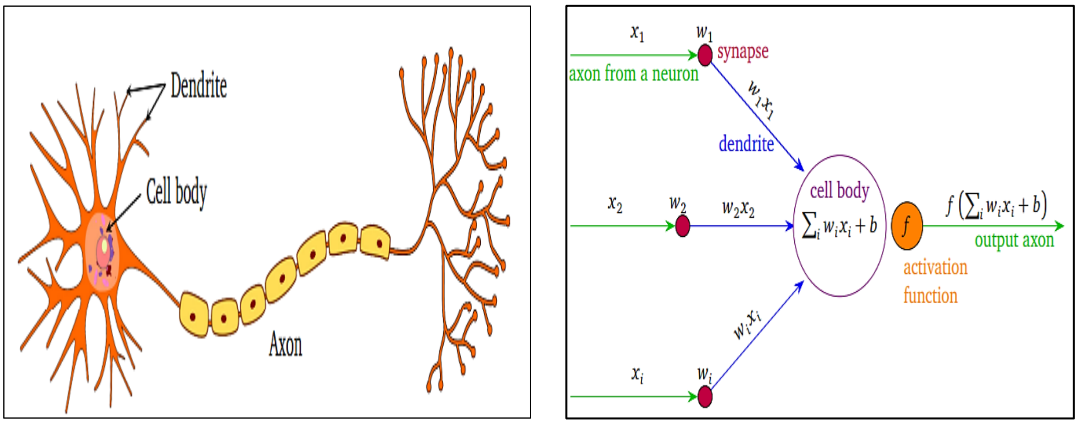

(a) Biological **(b)** Artificial

Figure 3. 3. Illustrations of (a) a biological and (b) The artificial model inspired by the biological neuron [70].

The technological development in the field of AI has expanded over time as shown in Fig. (3.4) [71].

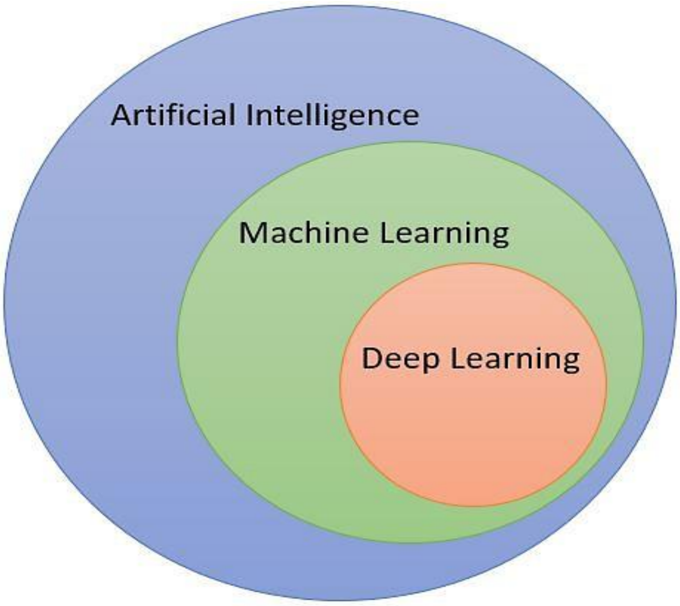

Figure 3. 4. Artificial intelligence development and expansion [71].

3.4.1. Learning Types of Neural Networks

There are four ways for learning neural networks: supervised, semi-supervised, unsupervised, and reinforcement learning. This thesis exclusively uses supervised learning, which is detailed in further depth in the section that follows. Semi-supervised and unsupervised are all covered in detail as follows [72].

1. Supervised Learning

Supervised learning which explains in Figure 3.5 is used when the data takes the form of input variables and output target values. The algorithm picks up the function for mapping input to output. It is a costly method for assignments when data is in short supply due to the availability of large-scale labeled data samples. These methods may be roughly classified into two groups:

- **Classification:** The output variable is one of a predetermined number of categories. For instance, “cat” or “dog”, “positive” or “negative”.

- **Regression**: The output variable might be either real or continuous. “Price” and “geographical location” are two examples.

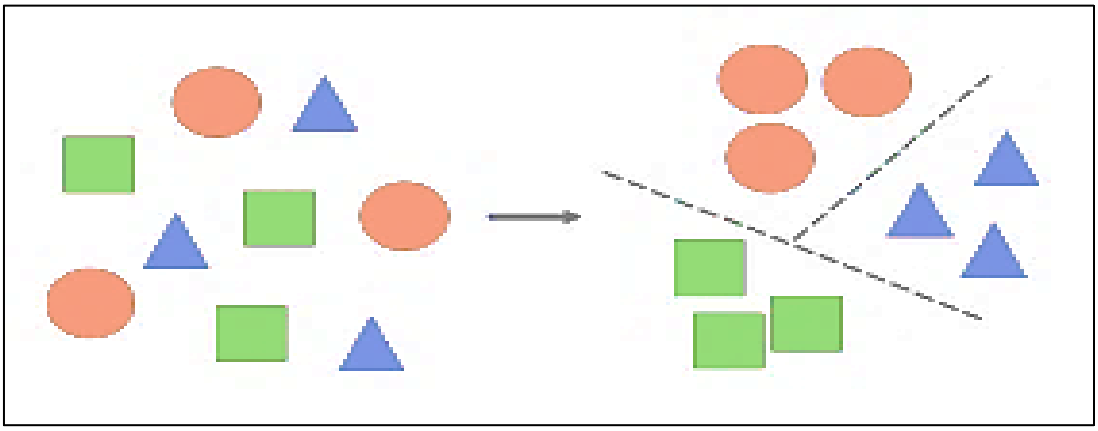

Figure 3. 5. Overview of supervised learning. Input examples are categorized into a known set of classes [72].

2. Unsupervised Learning

Unsupervised learning in Figure 3.6 is used when the data is only accessible as an input and there is no matching output variable. To learn more about the data’s features, such algorithms simulate the underlying patterns in it. Clustering is a common sort of unsupervised technique. This approach discovers intrinsic groupings in data and then uses them to predict output for unknown inputs. Predicting client purchase behavior is an example of this strategy.

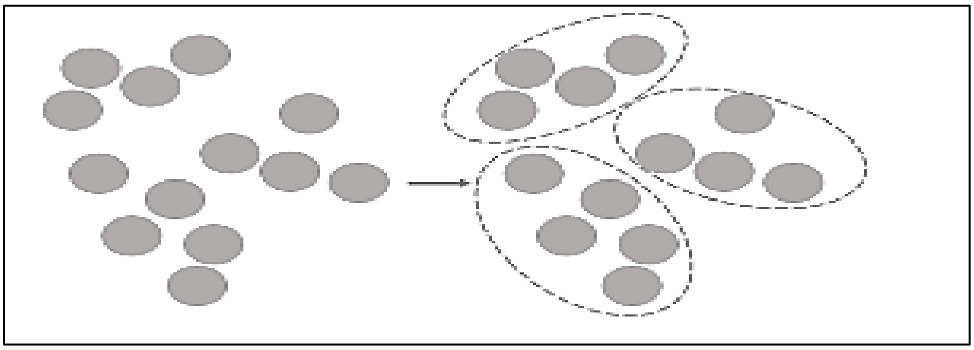

Figure 3. 6. Overview of unsupervised learning. Input samples are grouped into clusters based on the underlying patterns [72].

3.4.2. Sampling methods for dataset splitting

A more complicated sampling approach is necessary for generalization error when the size of the data collection is constrained. This is because dividing a small dataset into three pieces will almost always result in insufficient training data for improving a neural network. This issue may be resolved using a variety of resampling techniques. These methods split the data into training and testing divisions many times. A neural network is trained and tested for each partition, and the error rates are averaged. This provides a generalization error estimate for the neural network. K-fold cross-validation and random subsampling are the most often used approaches (also known as Monte Carlo cross-validation) [73]. The next subsection explains both ways.

1. K-fold Cross-Validation

The dataset of size N is randomly divided into K subsets, commonly known as folds, in K-fold cross-validation. These subsets are nearly equal in size and mutually exclusive. Figure 3.7 shows an instance of a K = 5 split. The error rate is measured using the k^{th} fold (k = 4) in Fig. (3.7), whereas the other K-1 folds are utilized for training. This is performed for k = {1, 2, ..., K} and the average of the K error rates are used to determine the generalization error. The bias-variance trade-off is controlled by the parameter K [2, N]. A small K leads to little training data and, as a result, significant bias with low variance. The variance grows but the bias reduces as K increases (to a maximum of K = N). Many studies indicate that selecting a favorable K (e.g., 5 or 10) results in acceptable trade-offs between bias and variance[74].

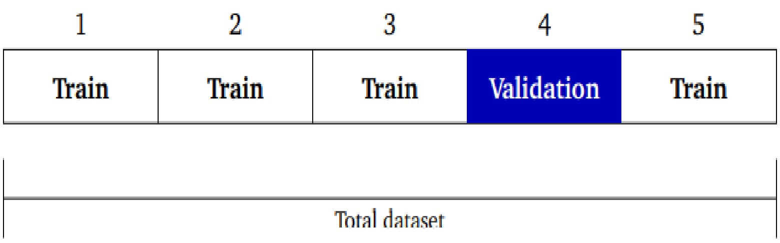

Figure 3. 7. Illustration of data splitting using K-fold cross-validation [74].

2. Random Subsampling

Random subsampling divides the dataset into a training and validation set, and it is frequently performed numerous times “I” to calculate the generalization error. The training set has n_t = N p samples, whereas the validation set has n_v = N- n_t samples. The bias-variance trade-off is controlled by the parameter p ∈ (0, 1). In each iteration, a new training validation partition is randomly picked from the dataset without replacement, and the error rate of the validation set is calculated. To determine the generalization error, all error rates are averaged. Figure 3.8, for example, shows a split of p= 70% and I = 30%. A big value for the parameter p results in less bias and more variation. Where the total dataset contains N samples [75].

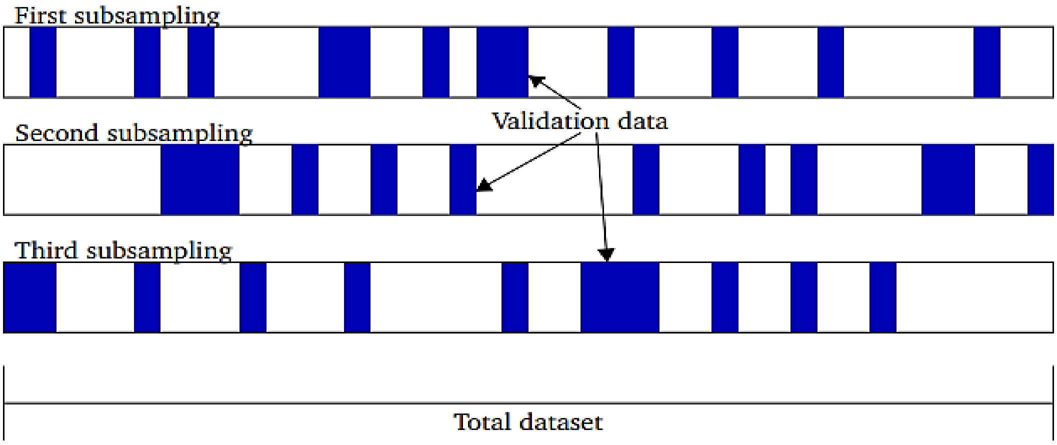

Figure 3. 8. Illustration of data splitting using the random subsampling approach which is repeated several times I [75].

3.5. MACHINE LEARNING AND DEEP LEARNING

Artificial intelligence (AI) has existed for many decades, and the field is wide. AI can be viewed as a set that contains machine learning (ML), and deep learning (DL). The ML is a subset of AI, meanwhile, DL is in turn a subset of ML.

3.5.1. Machine Learning (ML)

Machine Learning is not a new concept in the field of computer science. However, it is a phrase that is always developing and evolving. ML is the study of how to utilize machines to replicate human capacity and behavior. It is regarded as a technology that answers queries and generates meaning from data. It combines statistics and computer science to allow computers or machines to do certain tasks. Unlike humans, ML can learn and adapt more quickly. It is the subset of AI in which approaches, models, and algorithms are used to learn from data and information to extract knowledge, patterns, or offer AI applications. ML is made up of a collection of algorithms that are used to train the historical dataset and produce future predictions. Data is being generated at an increasing rate as a result of the advancement of technology and the internet, which means there is a massive amount of data for the machine to learn and evaluate [76].

3.5.2. Deep Learning (DL)

Deep learning was initially presented in 2006 as a new study topic in machine learning to understand data characteristics and find better data expression through multi-level structure and layer-wise training. The fundamental concept is to detect various types of data including images, text, voice, and so on to simulate the human brain's ability to learn new things using a multi-layer network structure. Deep learning, as opposed to typical machine learning approaches, may combine feature extraction and categorical regression into a single model, significantly reducing the labor of artificial feature construction. Based on their structures and uses, deep learning models may be divided into three types: generative deep architectures, discriminative deep architectures, and hybrid deep architectures. Deep generative architectures such as the Deep Boltzmann Machine (DBM) and Deep Belief Network (DBN) are used to represent high-level data correlation. To properly compute the both prior and posterior probability, the category of the observation samples is determined using a joint probability distribution. Convolutional Neural Networks (CNNs) are a common example of a discriminative deep architecture used in classification tasks to explain the posterior probability of data. Recurrent Neural Networks (RNN) are hybrid deep architectures that integrate characteristics from both generative and discriminative components. To simplify and optimize the overall model while addressing the classification issue, they make use of the output from the generative architecture. Deep learning has a stronger potential to extract contextual information and global features from the underlying characteristics of data, making it the method of choice for solving many complicated problems. Researchers have just completed an exceptional study on this topic, offering a large number of effective models that may be immediately used and improved based on particular requirements [77].

3.5.2.1. Convolutional Neural Networks (CNNs)

Convolutional Neural Networks (CNNs) are multi-layer perceptron-based discriminative classifiers. To put it another way, given labeled training samples, for the input data, the algorithm will evaluate the likelihood of each category being present. With minimal to no pre-processing, it aims to identify certain patterns straight from picture pixels. due to its ability to classify objects in a shift-invariant manner using a hierarchical framework. Convolutional layers, pooling layers, and fully-connected layers make up the majority of a complete CNN architecture, as seen in Figure 3.9 [78].

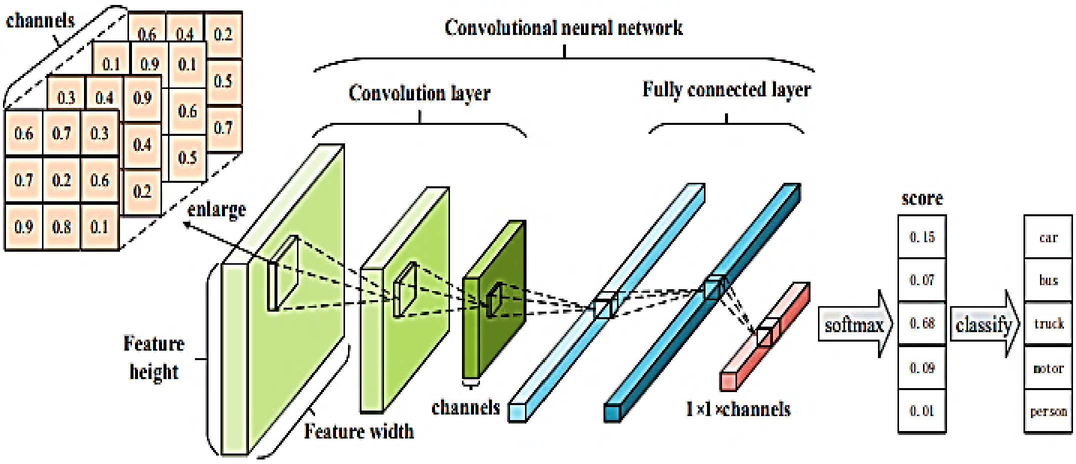

Figure 3. 9. A convolutional neural network (CNN) architecture [78].

1. **Convolutional layer**

A CNN model's brain is the convolutional layer, which employs convolution kernels to extract information from input images. The pixels of the next layer may be turned into a local receptive field, which is the connected area of any convolution kernel applied to the input data, using this method. To extract features, a type of linear process known as convolution is performed. It applies a little array of numbers known as a kernel to the input, which is a tensor array of numbers. A feature map, also known as an output value at the corresponding place of the output tensor, is obtained by computing and summing an element-wise product between each kernel element and the input tensor at each point of the tensor as shown in Figure 3.10 [79].

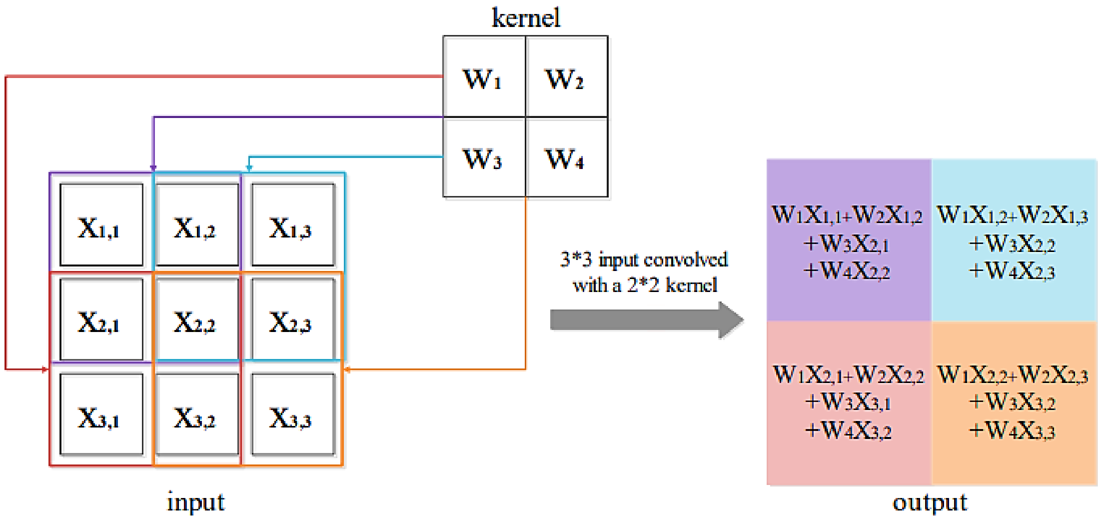

Figure 3. 10. Process of convolution [79].

2. **Pooling Layer**

Another important concept in CNN is the pooling layer, which is frequently added after the convolutional layer and offers a method of non-linear down-sampling. It divides the output of the convolutional layer into distinct areas and creates a single summary for each region to obtain the attributes of convolution. Max pooling, Average pooling, and stochastic pooling are examples of traditional pooling approaches. Fig. (3.11) depicts its operation principles. Average pooling averages all of the values in the local receptive region, whereas max-pooling takes the largest value in the local receptive zone. Stochastic pooling assigns a probability value to each sample point in the locally receptive region and then chooses a value at random based on those probabilities. Based on the demands, further pooling methods including adaptive pooling, mixed pooling, spectral pooling, spatial pyramid pooling, and so on are offered. The pooling procedure enhances the tolerance of distortion and displacement to improve fault tolerance by extracting the necessary characteristics from the local region. Furthermore, pooling minimizes the spatial size of data, improving computing efficiency [80].

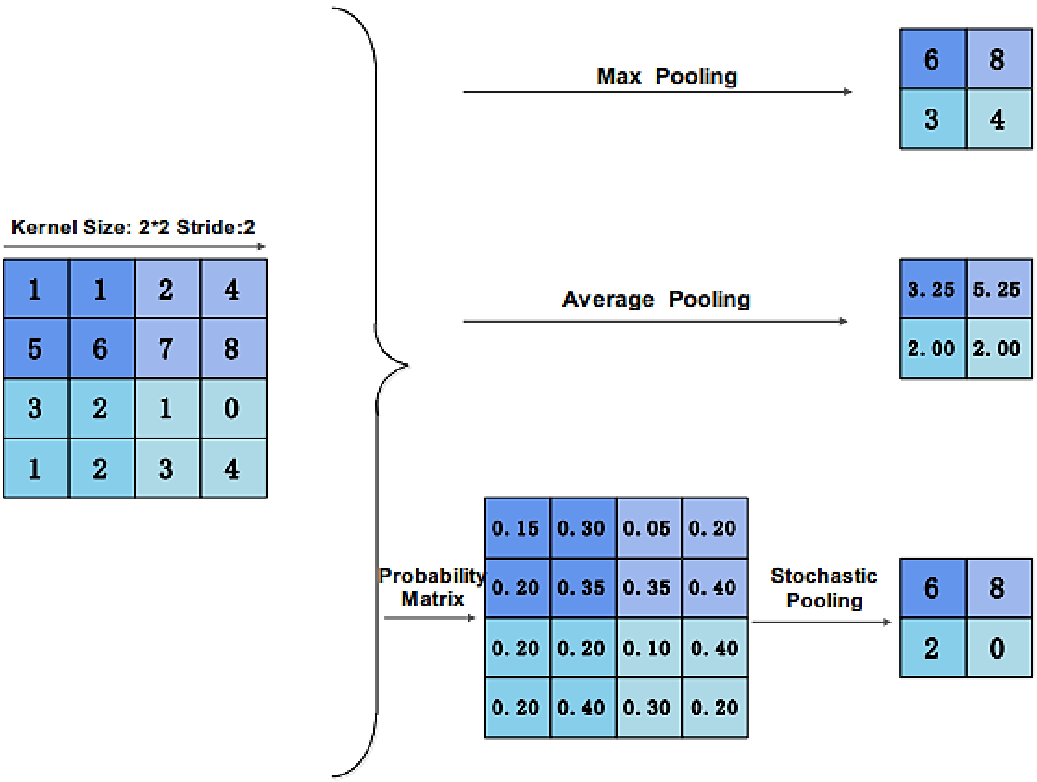

Figure 3. 11. Classic pooling working principles [80].

3. Nonlinearity Layer

The non-saturating activation function is used in this layer. While having no impact on the convolution layer's receptive fields, it will boost the nonlinear features of the choice function and the overall network that are desirable for multi-layer networks. The most commonly used functions are [81].

- **Rectified Linear Unit function (ReLU):** ReLU is the most used activation function for convolution layers. Eq. (3.17) provides a mathematical definition of it:

$$f(x) = max(0.x) = \begin{Bmatrix} 0 & if\ x < 0 \\ 1 & if\ x \geq 0 \end{Bmatrix} \tag{3.17}$$

- **LeakyReLU:** It is an effort to address the fading ReLU issue. Instead of the function being zero when x < 0, a leaky ReLU will have a little negative slope (of 0.01, or so). This is calculated using the function and is illustrated in Eq. (3.18), where is a tiny constant.

$$f(x) = 1(x < 0)(\alpha x) + 1(x >= 0)(x) \tag{3.18}$$

- **Sigmoid function:** Its contour resembles the form of a S. The function has a range of [0, 1], hence its output is a prediction of a probability. It has the following mathematical form in Eq. (3.19):

$$f(x) = \frac{1}{1+ e^{-x}} \tag{3.19}$$

- **Hyperbolic Tangent (tanh) function:** Tanh has a similar shape to Sigmoid, however, its range is [1, 1]. The benefit is that zero values will be mapped close to zero, whereas negative values will be mapped substantially negatively. It is mathematically defined in Eq. (3.20):

$$f(x) = \tanh(x) = \frac{2}{1+ e^{-2x}} - 1 \tag{3.20}$$

4. **Flattening Layer**

The pooling layer's output will be a matrix, which cannot be fed into the neural network. The flattening layer transforms the $n \times n$ matrix from the pooling layer into a n^2×1 matrix that can be input into the neural network [82].

5. Softmax Layer

This layer is generally used when the neural network must solve problems involving multiclass categorization. Typically, Softmax serves as the activation function for some output nodes. Each node in the output layer is given a probability using the Softmax function. These probabilities are multiplied by one. The neural network's forecast is represented by the node with the highest value. Backpropagation and forward propagation are used by both the ReLU layer and the Softmax layer to train the CNN. Mathematically, the softmax function can be defined as Eq. (3.21):

$$\sigma(z)_i = \frac{e^{zi}}{\sum_{j=1}^{k} e^{zi}} \tag{3.21}$$

where i= 1, 2, …, k and z=z_1, z_2,…, z_k. Eq. (3.21) shows the standard exponential function of each element z_i of the input vector Z and normalizes these values by dividing them by their sum. This normalization ensures that the sum of the components of the output vector σ(z) is 1 [82].

6. Dense layer

It is the regular deeply connected neural network layer. It is the most common and widely utilized layer. The dense layer performs the following operation on the input and returns the result. This layer formulates as Eq. (2.22) [83]

Output = activation (dot (input, kernel) + bias) (3.22)

7. Fully Connected Layer

One or perhaps more fully connected layers are frequently included right before the classification result in a CNN model. As with neural network layer architectures, a completely connected layer is made up of a fixed number of unconnected neurons, and neurons between neighboring layers are fully connected, as illustrated in Figure 3.12. This fully connected layer structure creates a shallow multi-layer perceptron that seeks to classify the input data by combining previously derived local feature information with categorical classification [84].

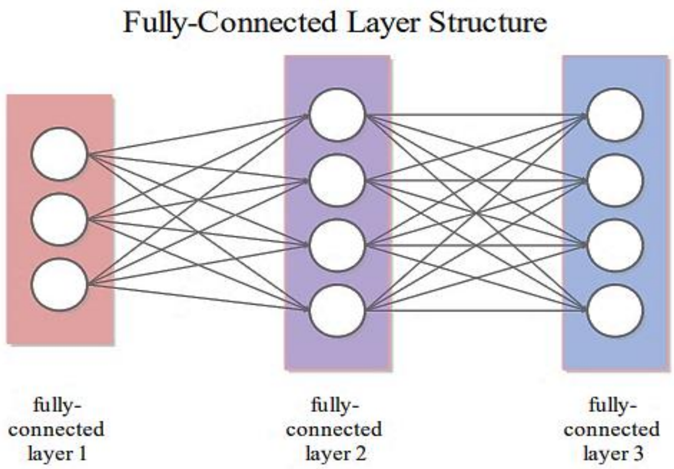

Figure 3. 12. Fully connected layer [84].

3.6.3. CNN-1D VS CNN-2D

According to much research, 1D CNNs are beneficial and hence superior to their 2D counterparts in dealing with 1D signals for the following reasons [85].

1. The computational difficulties of 1D and 2D convolutions differ significantly, i.e., an image with N×N dimensions convolving with K×K kernel would have a computational difficulty, but the corresponding 1D convolution will not (with the same dimensions, N and K). This suggests that the computational complexity of a 1D CNN is much lower than that of a 2D CNN under identical conditions (same design, network, and hyperparameters).
2. In general, most 1D CNN applications have utilized compact (with 1-2 buried CNN layers) setups with networks containing 10 K parameters, but practically all 2D CNN applications have employed "deep" architectures with more than 1 M (typically exceeding 10 M) parameters. Networks with shallow architectures are easier to train and implement.
3. Deep 2D CNN training typically necessitates the use of specialized hardware (e.g. Cloud computing or GPU farms). For training compact 1D CNNs with few

hidden layers (e.g., 2 or less) and neurons (e.g., 50), any CPU implementation on a typical computer is practical and relatively quick.

4. Compact 1D CNNs are highly suited for real-time and low-cost applications, particularly on mobile or handheld devices, because of their cheap processing needs.
5. Compact 1D CNNs have shown higher performance in situations with little labeled data and large signal fluctuations gathered from various sources (i.e., patient ECG, civil, mechanical, or aerospace structures, high-power circuitry, power engines or motors, etc.).

3.6. PERFORMANCE METRICS USED FOR DETECTION EVALUATION

The following matrices were used to evaluate the performance of the detection model [86].

3.6.1. Accuracy

The most important criterion for evaluating the performance of a convolutional neural network is accuracy. Accuracy is defined as the sum of true positive and true negative values divided by the total confusion matrix component. Eq. (3.23) is used to express it as follows:

$$\text{Accuracy} = \frac{\text{TP+TN}}{\text{TP+TN+FB+FN}} \tag{3.23}$$

3.6.2. Precision

Precision is a crucial metric for assessing the performance of CNN models. It keeps track of how many positive forecasts were correct. Precision is measured as the ratio of real positive anticipated components to the total number of positive predicted components. It is represented by Eq. (3.23) as follows:

$$\text{Precision} = \frac{\text{TP}}{\text{TP+FP}} \tag{3.24}$$

3.6.3. Recall (Sensitivity)

Another significant parameter for analyzing classifier performance is called recall. It is defined as the ratio of true positive anticipated components to the sum of true positive predicted components and false negative predicted components. Eq. (3.25) is used to express it as follows:

$$\text{Recall} = \frac{\text{TP}}{\text{TP}+\text{FN}} \tag{3.25}$$

3.6.4. F1-score

The F1 score is an important metric for determining test accuracy. It is the arithmetic mean of precision and recall. It is defined as the ratio of the multiplication of precision and recall to the total of precision and recall multiplied by two. Eq. (3.26) is used to express it as follows:

$$\text{F}_1 = 2 * \frac{\text{precision} * \text{recall}}{\text{precision}+\text{recall}} \tag{3.26}$$

Where,

TP = The number of instances that were predicted to be positive but ended up being true is known as the true positive rate.
FP = False positives are instances where results were anticipated to be positive but ended up being negative.
TN = The number of cases that were predicted to be negative but ended up being true is known as the real negative rate.
FN = False negatives are instances where results were anticipated to be negative but ended up being positive.

PART 4

THE PROPOSED SYSTEM

The steps used to attain the key goals of this thesis are discussed in this chapter. This includes a preprocessing and feature reduction step before the system predicts respiratory diseases using the proposed deep Convolution Neural Networks (CNN) model. This system’s architecture is shown first. The classification model is next discussed, followed by data pre-processing to prepare data for the following operations.

4.1. THE PROPOSED SYSTEM

The suggested approach which is depicted in Fig. (4.1) designed to detect infection with respiratory disorders utilizing X-ray images from a COVID-19 Radiography dataset. The dataset is divided into two parts using the random subsampling method into two parts, the first is 70%, and this data is used to train the proposed neural network, while the remaining 30% of the data is used to test the system at a later stage. The suggested system has several stages in which the images are processed in various ways and subsequently the features are reduced in multiple methods, such as LDA and GLCM. The suggested Convolutional Neural Network (CNN) is then used as the final stage in the system to differentiate patients with (COVID-19, Viral Pneumonia, or Lung Opacity) from healthy people, and the system is evaluated using a set of assessment criteria. In this section, we will go over these stages in further detail.

4.1.1. The Proposed System Requirements

The proposed system necessitates the following hardware and software to achieve its goal:

4.1.1.1. Software Requirements

The proposed system was compatible with Microsoft Windows 10. To create the suggested system there are a set of programming languages was used:

- Python with IDLE (Python 3.6 64-bit)
- C++ with Visual Studio 2013
- Java with NetBeans IDE 8.2
- Oracle

4.1.1.2. Hardware Requirements

This work is completed on a Lenovo ThinkPad computer that meets the following requirements:

- Intel(R) Core(TM) i5-10210U CPU @ 1.60GHz 2.10 GHz
- RAM 8.00 GB
- Operating system: 64-bit

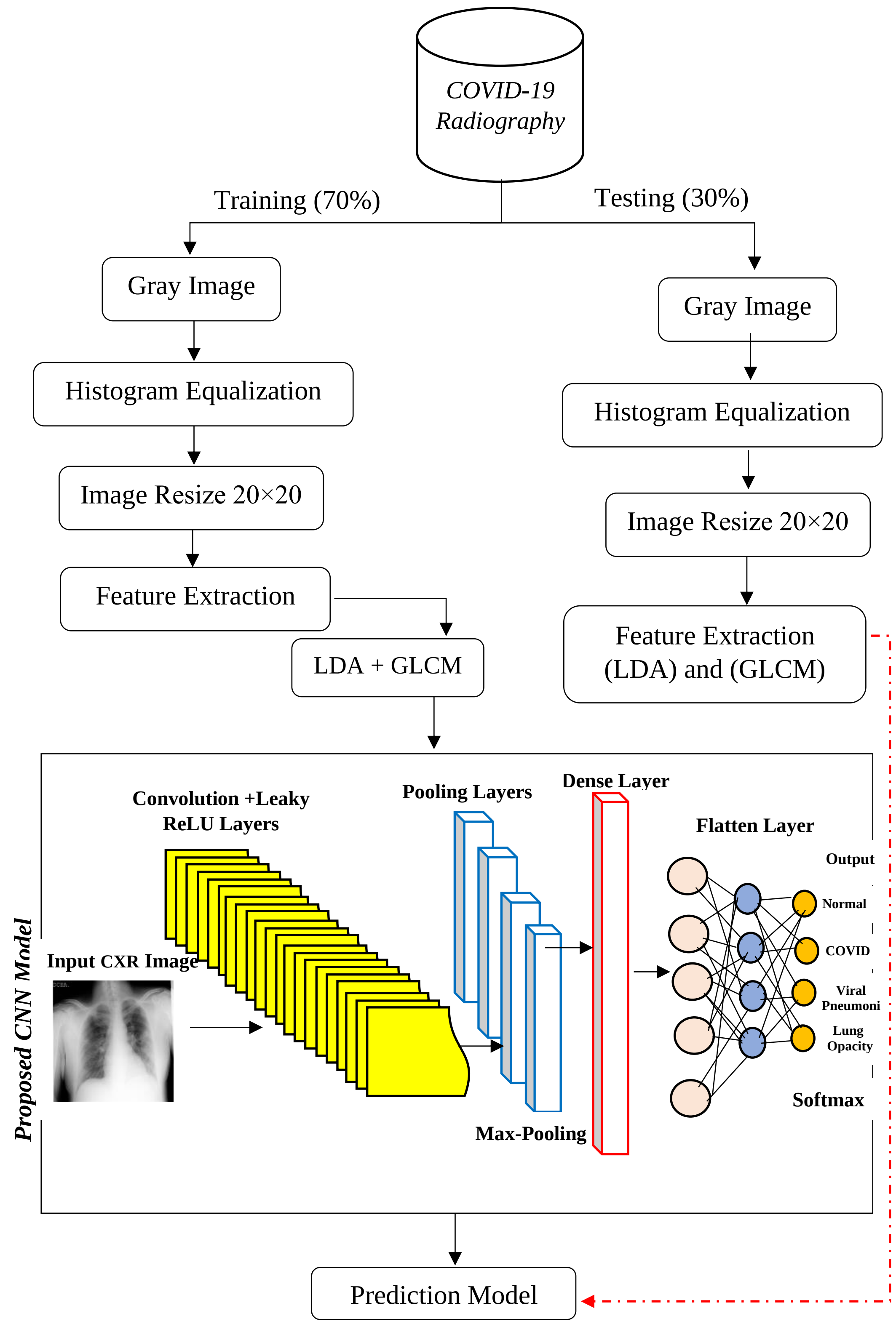

Figure 4.1. The proposed respiratory disease detection system is based on CNN.

4.1.2. Splitting of COVID-19 Radiography Dataset Stage

The random sampling method was employed to ensure correct generalization while limiting overtraining. The COVID-19 Radiography dataset was split into two subsets: one for training (70%) and one for testing (30%) the final model results. The algorithm (4.1) describes this technique's characteristics in detail.

Algorithm (4.1). COVID-19 Radiography Dataset Splitting

Input: AD dataset

Output: Splitting dataset (70% for training, 30% for testing)

Begin

```
Create a list of model parameter values to be assessed
    For each parameter set do
        For each resampling iteration do
            Random specific samples
            Model the remaining data and fit it
            Assume the samples
        End for
    Find the random forecasts' average performance.
    End for
    Identify the ideal parameter set.
    Fit the final model to each training batch of data using the
    ideal parameter set.
```

End

4.1.3. Preprocessing Stage

Data may be thought of as the model algorithm quickly analyzing the aspects of the data. Data pre-processing is the most crucial and crucial phase for a deep learning algorithm to perform well in terms of generalization. There are the following supporting procedures in this stage:

- **Transform the Image to Grayscale**

The input image is color transformed from an RGB color space impersonation to a grayscale color space. In comparison to a color image, switching to grayscale requires only 1/4 of the data to be processed. Because of this data reduction, the technique can be executed in a reasonable amount of time for many image-processing applications. The resulting grayscale image, on the other hand, must retain all of the essential image information without loss. The algorithm (4.2) depicts the mechanics of this process.

Algorithm (4.2). Grayscale Transformation

Input: RGB X-ray image
Output: Grayscale X-ray image
Begin
1: Read an input image.
2: **For** each pixel in the image:
3: Extract its R, G, and B components
4: Convert to corresponding grayscale luminance, Call Eq. (3.1).
5: Put the grayscale luminance in the image at the position of the old Pixel.
6: **End for**
End

- **Apply Histogram Equalization**

The goal of histogram equalization is to evenly spread the contrast of a given image across the entire possible dynamic range, which in this example is between 0 and 1. Histogram equalization is one of the pixel brightness transformation algorithms. Because of its capacity to operate on practically any image, it's a well-known contrast enhancement technique. The details of histogram equalization are explained in Algorithm (4.3).

Algorithm (4.3). Histogram Equalization

Input: Grayscale image of X-ray image

Output: Grayscale of X-ray image with enhanced contrast

Begin

1: Get the input image with M*N size, gray level from 0 to 255.

2: Compute the histogram of pixel values of the input image. The histogram places the value of each pixel $f\ [x, y]$ into one of L uniformly-spaced buckets $h[i]$, Call Eq. (3.7), Where L=$\mathbf{2^8}$ and the image dimension is $M{\times}N$.

3: Calculate the cumulative distribution function, Call Eq. (3.8).

4: Scale the input image using the cumulative distribution function to produce the output image, Call Eq. (3.9).

5: Create a new image by replacing the original gray values with the new gray values.

End

- **Resize Image Process**

Finally, the image will be scaled to (20×20) dimensions. Bi-linear interpolation is defined as linear interpolation in two directions. As a result, the output is determined by taking the weighted average of the four closest neighbors. The operation is described in depth in Algorithm (4.4).

Algorithm (4.4). Bi-Linear Interpolation

Input: Grayscale of X-ray image with enhanced contrast

Output: Resized X-ray image

Begin

1: Read the input image.

2: While not (EOF) do:

Algorithm (4.4). Bi-Linear Interpolation

3: Extract the points Q_{11}, Q_{21}, Q_{12}, and Q_{22} points, which are the position of points.

4: Extract the (x_1, y_1) and (x_2, y_2) coordinates.

5: Calculate R_1, Call Eq. (3.10).

6: Calculate R_1, Call Eq. (3.11).

7: Calculate P, Call Equation (3.12).

8: End While

End

4.1.4. Feature Extraction Stage

Feature reduction sometimes referred to as dimensionality reduction, is the process of reducing the number of features in a computation that consumes a lot of resources without giving up important information. As the number of qualities drops, so do the variables, making the computer's job simpler and quicker. Feature selection and feature extraction are the two steps in feature reduction. There are a variety of methods for feature reduction. These strategies were used by this system:

- **Extract Features of X-ray Images based on LDA**

The main purpose of LDA is to find a linear transformation that separates feature clusters the most after the transformation, which can be accomplished by examining the scatter matrix. The primary goal of this procedure is to increase inter-class scatter matrix estimation while decreasing within-class scatter matrix calculation. Algorithm explains LDA in detail (4.5).

Algorithm (4.5). Linear Discriminant Analysis (LDA)

Input: Resized X-ray image

Output: Feature Vectors

Begin

1: Read the X-ray image pixel by pixel.

2: For each class in the dataset, calculate the d-dimensional mean vectors.

3: Determine the scatter matrices (in-between-class and within-class scatter matrices).

4: Calculate the eigenvectors ($\boldsymbol{e_1}$,$\boldsymbol{e_2}$,...,$\boldsymbol{e_d}$) with corresponding eigenvalues ($\boldsymbol{\lambda_1}$,$\boldsymbol{\lambda_2}$,...,$\boldsymbol{\lambda_d}$) for the scatter matrices.

5: Order the eigenvectors using to decrease eigenvalues and select k eigenvectors that have the highest eigenvalues to create a d × k dimensional matrix W. (each column represents an eigenvector).

6: Utilize this d × k eigenvector matrix to transform the samples onto a new subspace. This can be shortened by the matrix multiplication: Y=X×W (where X represents n × d-dimensional matrix that represents the n samples, and y represents the transformed n×k-dimensional samples in a new subspace).

7: Return feature vectors.

End

- **Extract Features of X-ray Images based on GLCM**

The GLCM functions characterize an image's texture by calculating the frequency with which pairs of pixels with given values and in a specified spatial relationship occur in an image, generating a GLCM, and then extracting statistical measures from this matrix. The algorithm (4.6) depicts GLCM in detail.

Algorithm (4.6). Gray-Level Co-Occurrence Matrix (GLCM)

Input: Resized X-ray image

Algorithm (4.6). Gray-Level Co-Occurrence Matrix (GLCM)

Output: Feature Vectors

<u>**Begin**</u>

1: Read the X-ray image pixel by pixel.

2: For each class in the dataset, calculate the d-dimensional mean vectors.

3: Consider a matrix A of size 5×5 of an input image.

4: Define the quantization level as 8 and displacement or offset (between the two pixels) as 1.

5: Initialize the GLCM matrix of size 8×8 with zeros.

6: Start transferring from the first element of matrix A and its adjacent element and increment the GLCM matrix at row 1 and column 2 by 1.

7: Move to the next element of matrix A and its adjacent element and increment the GLCM matrix at row 2 and column 3 by 1.

8: Move to the next element of matrix A and its adjacent element and increment the GLCM matrix at row 3 and column 2 by 1.

9: The final GLCM matrix after transferring all the elements in matrix A.

<u>**End**</u>

4.1.5. Classification Stage

In this section, the suggested CNN model for respiratory disease classification is explained. In this method, the proposed CNN model is used to classify data immediately after the dataset is loaded, split, processed, and the feature were extracted from them. Algorithm (4.7) illustrates this model in more detail. The proposed CNN model consists of 28 layers as follows:

- Convolutional Neural Network (CNN) (8) layers.
- Leaky ReLU (8) layers.
- Max Pooling (8) layers.
- Flatten (1) layer
- Dense (3) layer.

These layers are described in more depth in Table 4.1.

Table 4. 1. The proposed CNN layers.

NO.	Layer Type	Filters	Size/Stride	Activation Function
1	Convolutional	16	3/1	–
2	Leaky ReLU	–	–	–
3	Max Pooling	–	1/1	–
4	Convolutional	32	3/1	–
5	Leaky ReLU	–	–	–
6	Max Pooling	–	1/1	–
7	Convolutional	32	3/1	–
8	Leaky ReLU	–	–	–
9	Max Pooling	–	1/1	–
10	Convolutional	128	3/1	–
11	Leaky ReLU	–	–	–
12	Leaky ReLU	–	–	–
13	Max Pooling	–	1/1	–
14	Dense	–	–	Linear
15	Convolutional	256	3/1	–
16	Leaky ReLU	–	–	–
17	Max Pooling	–	1/1	–
18	Convolutional	512	3/1	
19	Leaky ReLU	–	–	–
20	Max Pooling	–	1/1	–
21	Convolutional	1024	3/1	
22	Leaky ReLU	–	–	–
23	Max Pooling	–	1/1	–
24	Dense	–	–	Linear
25	Convolutional	50	3/1	Linear
26	Max Pooling	–	1/1	–
27	Flatten	–	–	–
28	Dense	–	–	Softmax

Algorithm (4.7). The proposed CNN classification model

Input: COVID-19 radiography dataset.

Output: Accuracy of proposed CNN classification model.

<u>Begin</u>

1: Load the COVID-19 radiography dataset.

2: Splitting dataset, Call Algorithm (4.1).

3: Transform the image to grayscale, Call Algorithm (4.2).

4: Apply histogram equalization, Call Algorithm (4.3).

5: Resize images, Call Algorithm (4.4).

6: Extract features using two techniques:

- LDA feature extraction method, Call Algorithm (4.5).
- GLCM feature extraction method, Call Algorithm (4.6).

7: **Training dataset:**

Build the classification CNN model with the following layers:

- Layer 1 of the convolutional layer has a kernel size of 3, padding of 1, stride of 1, and filter number 16.
- Layer 2 with an alpha of 0.3 uses a leaky ReLU.
- Layer 3 is the maximum layer for pooling, with a pool size of 1, and a stride of 1.
- Layer 4 of the convolutional layer has a kernel size of 3, padding and stride of 1, and filter number 32.
- Layer-5 with an alpha of 0.3 uses a leaky ReLU.
- Layer 6 is the maximum pooling layer, and the pool size and stride are both 1.
- The layer 7 convolution layer has a kernel size of 3, padding equals 1, stride equals 1, and filter number 32.
- Layer-8 with an alpha of 0.3 uses a leaky ReLU.
- Layer 9 is the maximum pooling layer, and the pool size and stride are both 1.
- Layer 10 of the convolutional layer has a kernel size of 3, padding of 1, stride of 1, and filter number 128.
- Layer 11 is leaky ReLU has an alpha value of 0.3.

- Layer 12 is leaky ReLU has an alpha value of 0.3.
- The maximum pooling layer is layer 13, the pool size is 1, and the stride is 1.
- Layer 14 is a dense layer with a linear activation function.
- Layer 15 in the convolution stack has a kernel size of 3, padding of 1, stride of 1, and filter number 256.
- Layer-16 with an alpha of 0.3 uses a leaky ReLU.
- The layer-17 maximum pooling layer has a pool size of 1 and a stride of 1.
- The convolution layer is layer-18 with a kernel size of 3, padding of 1, a stride of 1, and filter of 512.
- Layer 19 is leaky ReLU, with an alpha value of 0.3.
- Layer 20 is the maximum pooling layer, with a pool size of 1 and a stride of 1.
- The convolution layer, layer-21, has a kernel size of 3, padding of 1, stride of 1, and filter number 1024.
- ReLU that is leaking, layer-22, alpha=0.3.
- Layer-23 with a pool size of 1 and a stride of 1 is the maximum layer for pooling.
- Layer 24 is a dense layer with a linear activation function.
- The convolution layer is represented by layer 25 with a kernel size of 3, padding of 1, stride of 1, and filter number 50.
- The maximum layer for pooling is layer 26, with a pool size of 1 and stride of 1.
- Flatten layer as layer-27.
- Layer 28 is a dense layer with softmax activation.

8: Test the remainder of the data that have been entered for training.

9: Return (accuracy)

<u>End</u>

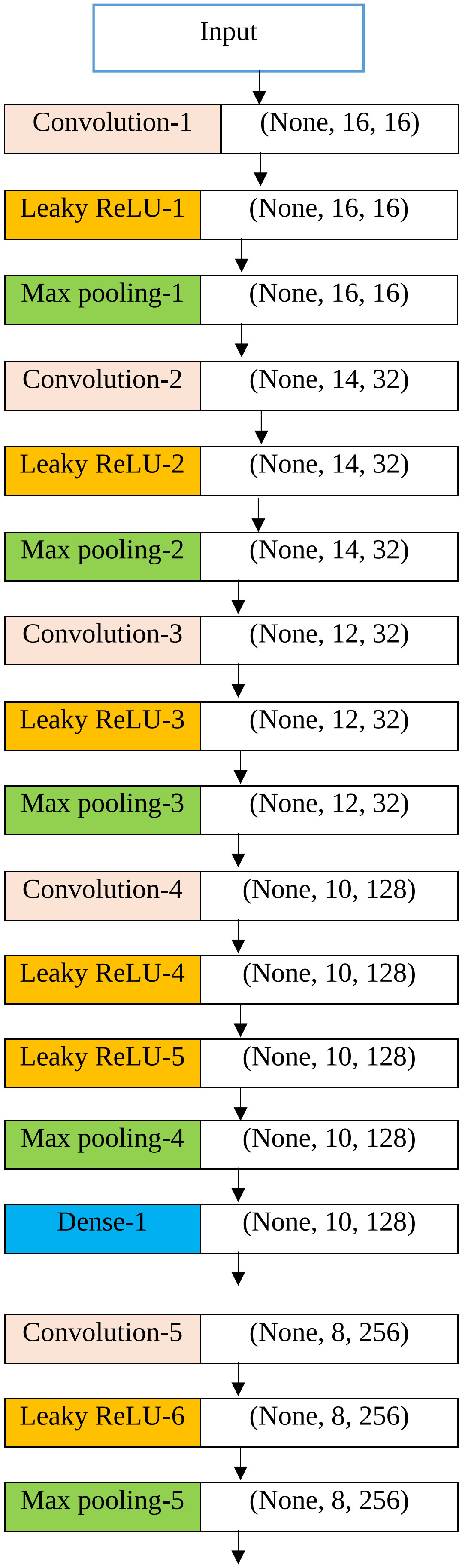
Input
Convolution-1
(None, 16, 16)
Leaky ReLU-1
(None, 16, 16)
Max pooling-1
(None, 16, 16)
Convolution-2
(None, 14, 32)
Leaky ReLU-2
(None, 14, 32)
Max pooling-2
(None, 14, 32)
Convolution-3
(None, 12, 32)
Leaky ReLU-3
(None, 12, 32)
Max pooling-3
(None, 12, 32)
Convolution-4
(None, 10, 128)
Leaky ReLU-4
(None, 10, 128)
Leaky ReLU-5
(None, 10, 128)
Max pooling-4
(None, 10, 128)
Dense-1
(None, 10, 128)
Convolution-5
(None, 8, 256)
Leaky ReLU-6
(None, 8, 256)
Max pooling-5
(None, 8, 256)

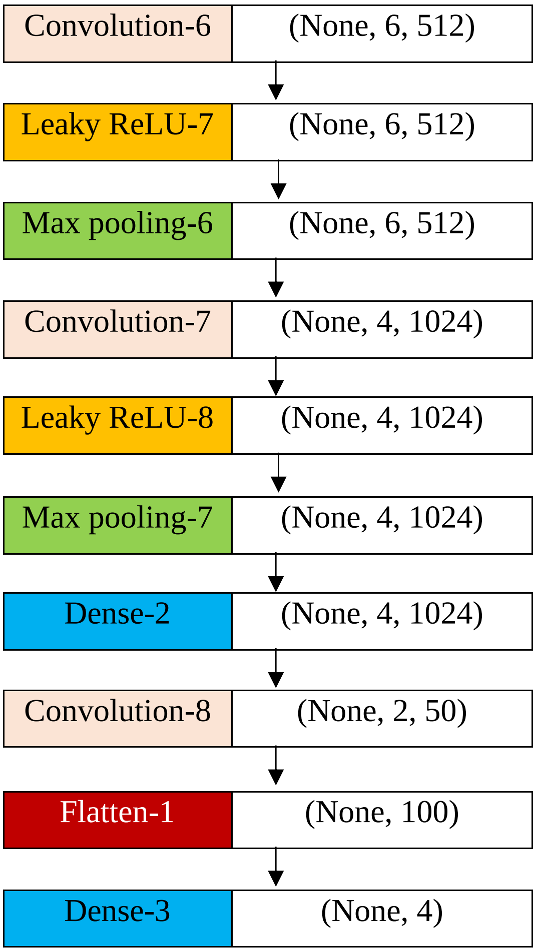

Figure 4. 1. Detail of the proposed CNN layers.

PART 5

RESULTS AND DISCUSSION

The suggested system presented in chapter 3 was used to carry out the research goals specified in that chapter. The research needs are addressed after a brief introduction to the Covid-19 Radiography dataset. The outcomes of the experiment are then listed and discussed in the following section.

5.1. DATASET DESCRIPTION

A study team from Qatar University in Doha, Qatar, and the University of Dhaka in Bangladesh has built a database of chest X-ray images for COVID-19-positive patients, as well as photos of normal and viral pneumonia, in collaboration with researchers from Pakistan and Malaysia. This COVID-19, normal, and other lung infection dataset. I made it balanced using augmentation and obtained balanced data. And we used the resulting data to test the proposed system, The COVID-19 Radiography Dataset is described in full in Table 5.1. Figures 5.1 to 5.4 show CXR images of COVID and normal patients from this sample.

Table 5. 1 COVID-19 Radiography dataset categories.

Category	No. of Chest X-ray (CXR) Images	
	Without augmentation	**With augmentation**
COVID-19	3616	10,000
Normal	10,192	10,000
Viral Pneumonia	1345	10,000
Lung Opacity (Non-COVID lung infection)	6012	10,000

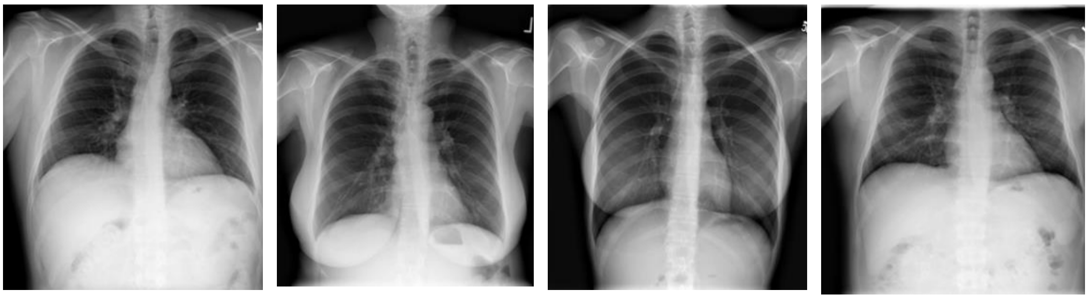

Figure 5. 1. Normal CXR image example from the COVID-19 Radiography Database.

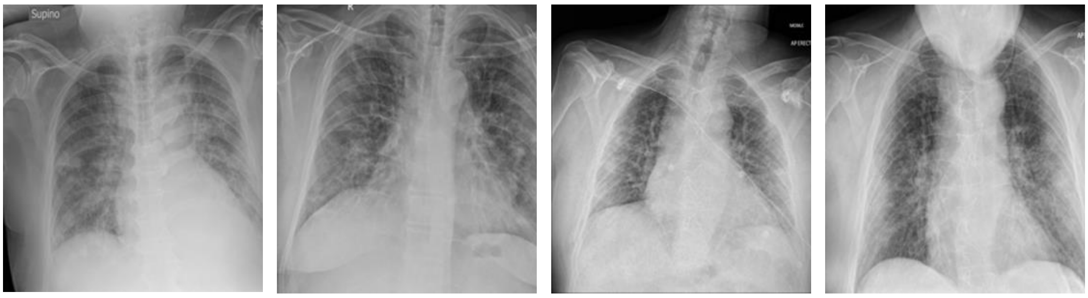

Figure 5. 2. COVID CXR image example from the COVID-19 Radiography Database.

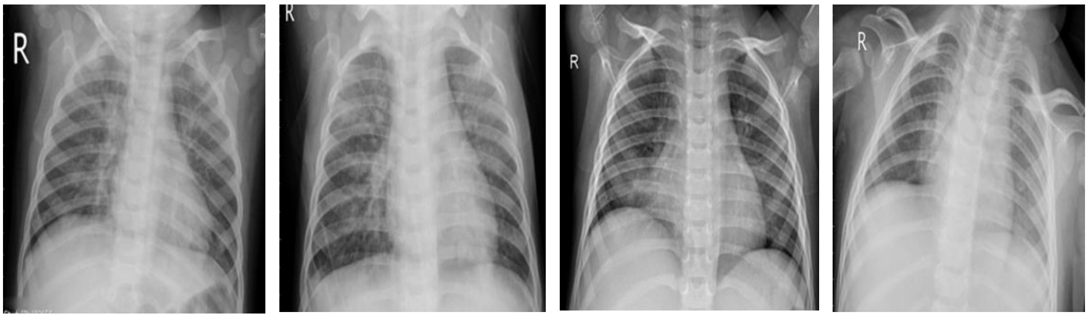

Figure 5. 3. Viral Pneumonia CXR image example from the COVID-19 Radiography Database.

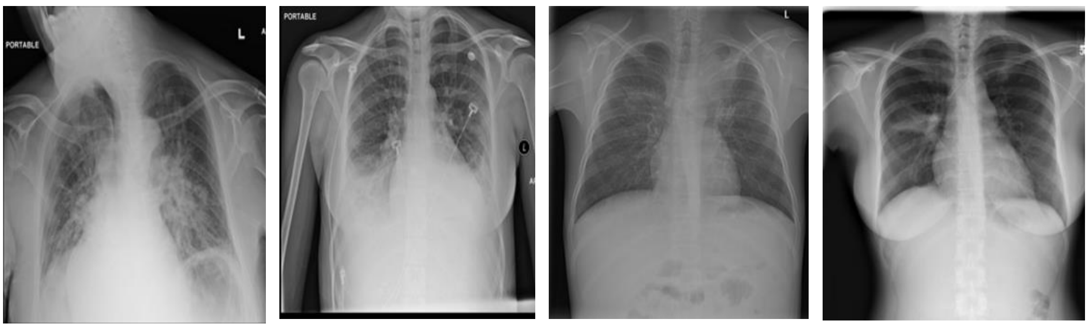

Figure 5. 4. Lung Opacity CXR image example from the COVID-19 Radiography Database.

5.2. RESULTS OF THE PROPOSED SYSTEM

This section explains the outcomes of the proposed respiratory disease stage system. Following the experiment, it was discovered that a ratio of 70% for the training set and 30% for the testing set is the best strategy, and after pre-processing the data set and decreasing the features using the previously discussed procedures, and the classification model employed as follows:

5.2.1. The Result of Grayscale Transformation and Histogram Equalization and Image Resize

In this section, a set of images are presented as samples of the dataset that was used after applying each of the two pre-processing processes, which are the process of converting the original image to grayscale and histogram equalization as shown in Figures 5.5 to 5.10 below. The image resizes to (20×20) example shown in Figure 5.11.

a. Original image **b.** Grayscale image **c.** Histogram equalization

Figure 5. 5. Preprocessing operations on the 1st sample of the dataset.

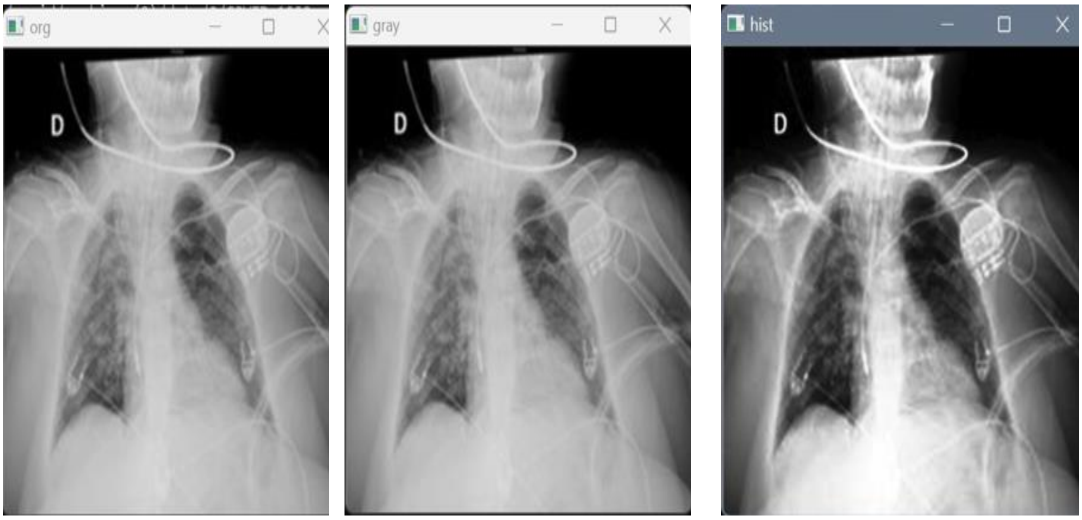

a. Original image **b.** Grayscale image **c.** Histogram equalization

Figure 5. 6. Preprocessing operations on the 2nd sample of the dataset.

a. Original image **b.** Grayscale image **c.**Histogram equalization

Figure 5. 7. Preprocessing operations on the 3rd sample of the dataset.

a. Original image **b.** Grayscale image **c.**Histogram equalization

Figure 5. 8. Preprocessing operations on the 4th sample of the dataset.

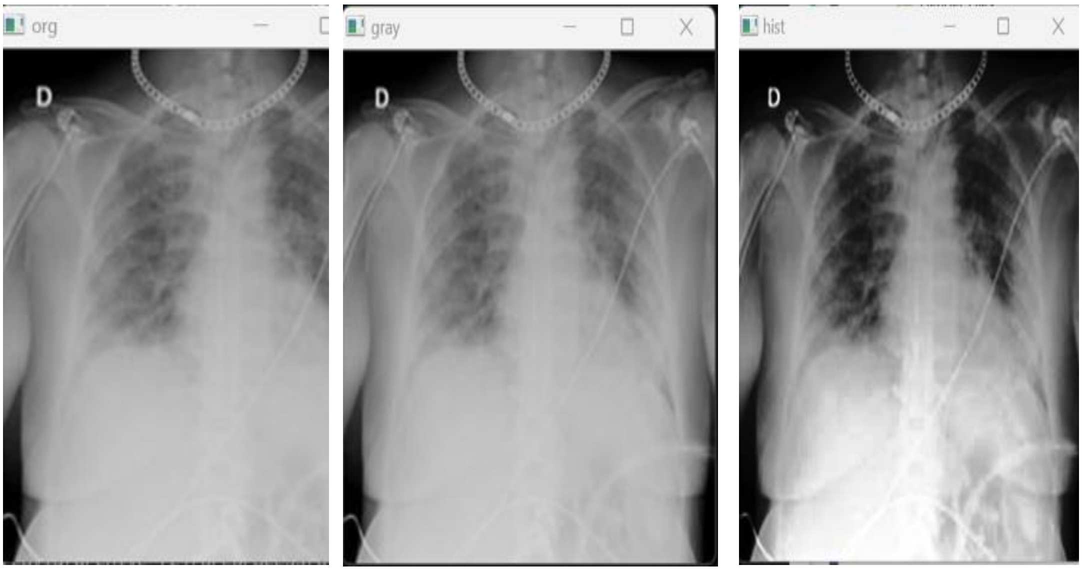

a. Original image **b.** Grayscale image **c.**Histogram equalization

Figure 5. 9. Preprocessing operations on the 5th sample of the dataset.

a. Original image **b.** Grayscale image **c.**Histogram equalization

Figure 5. 10. Preprocessing operations on the 6th sample of the dataset.

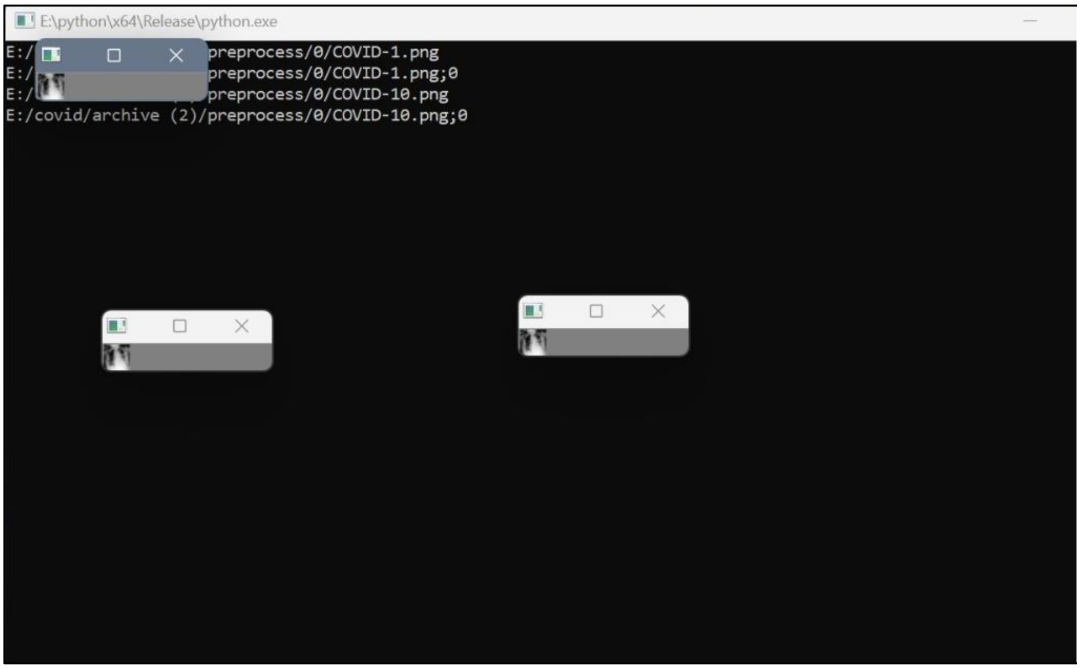

Figure 5. 11. Image resize operation.

5.2.2. Result of Feature Extraction

After performing pre-processing operations on the images, the features are extracted from the image using two techniques LDA and GLCM as shown in Figure 5.12.

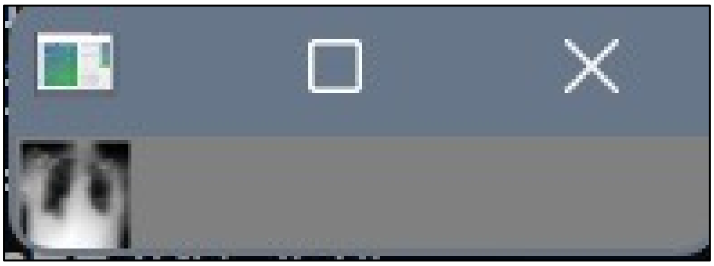

Figure 5. 12. GLCM features.

5.2.3. Results of the Classification Using the Proposed CNN

The results were determined using the number of metrics discussed in the second chapter of this thesis. The results are shown in Table 5.2, and the chart is explained in Figure 5.13.

Table 5. 2. Results of the proposed CNN classification model.

	Accuracy	**Precision**	**Recall**	**F-score**
The proposed CNN model	99.94%	100%	100%	100%

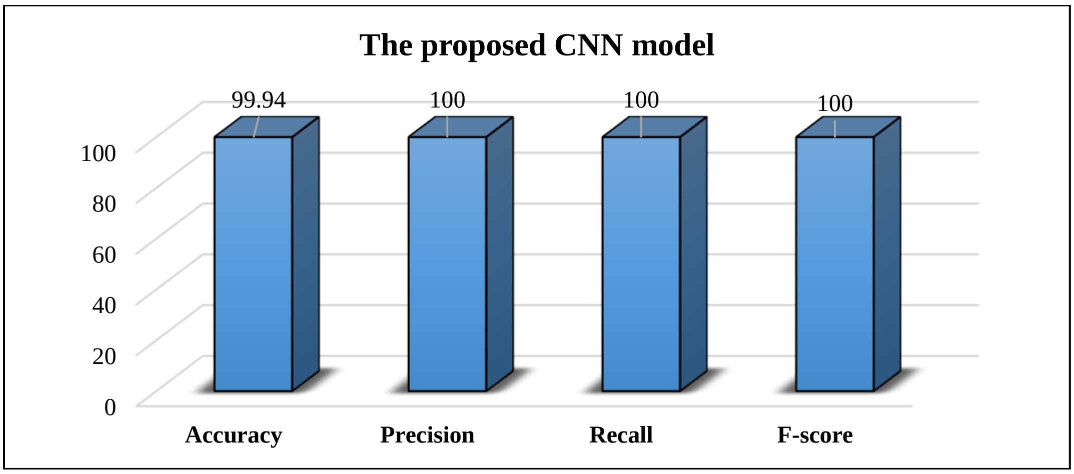

Figure 5. 13. Chart of first CNN classification model results.

5.2.4. Comparison Results with Related Studies

Several studies have been done in recent years to determine and classify respiratory diseases depending on the convolution neural network. Researchers are looking for a more effective solution to this challenge. We compared our suggested model with previous studies. The comparison results are shown in Table 5.3.

Table 5. 3. Comparison results on COVID-19 Radiography with related studies.

Ref. No.	Technique	Accuracy	Precision	Recall	F-score
[26]	CNN	98%	98.2%	97%	98%
[27]	CNN	96%	96%	94%	96%
[28]	CNN	94.64%	96.52%	96.50%	94.63%
[29]	CNN	96%	97.27%	92.64%	96%
[30]	CNN	96.4%	96.5%	96.2%	95.9%
[31]	CNN	98%	99%	100%	99%
[32]	CNN	98%	96.4%	100%	97.9%
[33]	CNN	99.06%	99.07%	99.06%	99.06%
[34]	CNN	99%	99%	99%	99%
[35]	CNN	99.17%	99.31%	99.03%	99.17%
[36]	CNN	94.2%	94.4%	94.2%	94.2%
[37]	CNN	94%	90%	90%	90%
[38]	CNN	99.68%	99.66%	99.66%	99.65%
[39]	CNN	93.75%	95.45%	100%	93.70%
[40]	CNN	98.43%	98.26%	99%	98.43%
[41]	CNN	99.9%	99.89%	99.9%	99.9%
[42]	CNN	97%	97.2%	98%	97.67%
[43]	CNN	87.66%	88.21%	87.34%	87.65%
[44]	CNN	93.91%	93.89%	93.99%	93.92%
[45]	CNN	98.40%	98.34%	98.56%	98.41%
[46]	CNN	99.8%	98%	98.5%	99.8%
Our Proposed Method	**Proposed COVCNN**	**99.94%**	**100%**	**100%**	**100%**

According to the table above, the suggested CNN model outperformed the other models in detecting respiratory infection using the identical COVID-19 Radiography dataset. The proposed system aids in early and accurate detection, improving the probability of treatment and the number of recoveries from these disorders. Figures 5.14 - 5.17 illustrate the accuracy, precision, recall, and f-score comparison with related studies, accordingly.

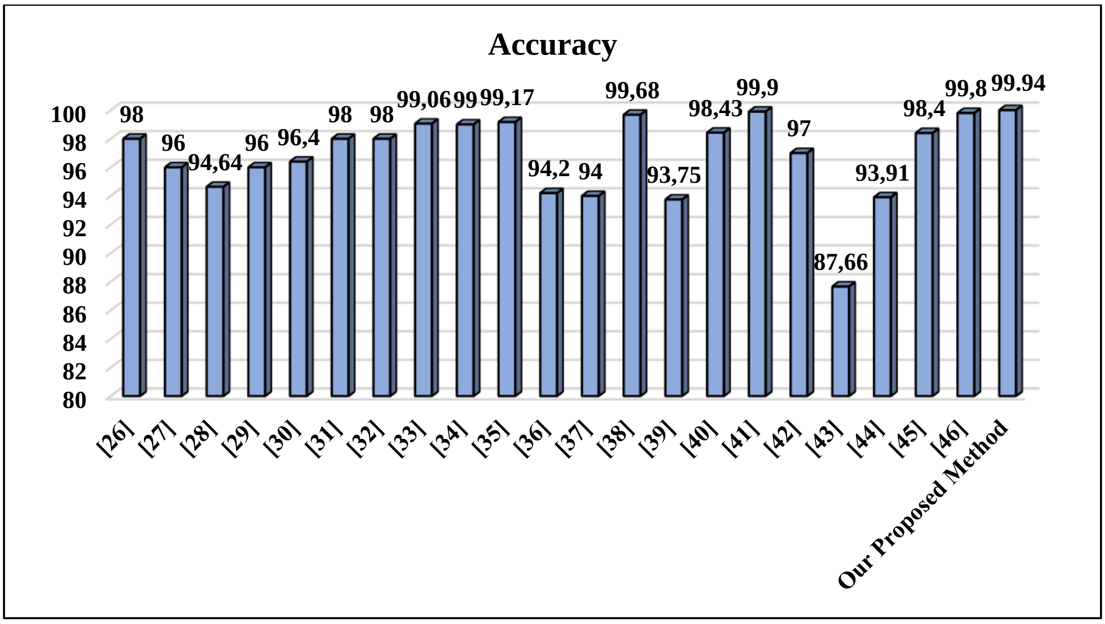

Figure 5. 14. Accuracy's results comparison.

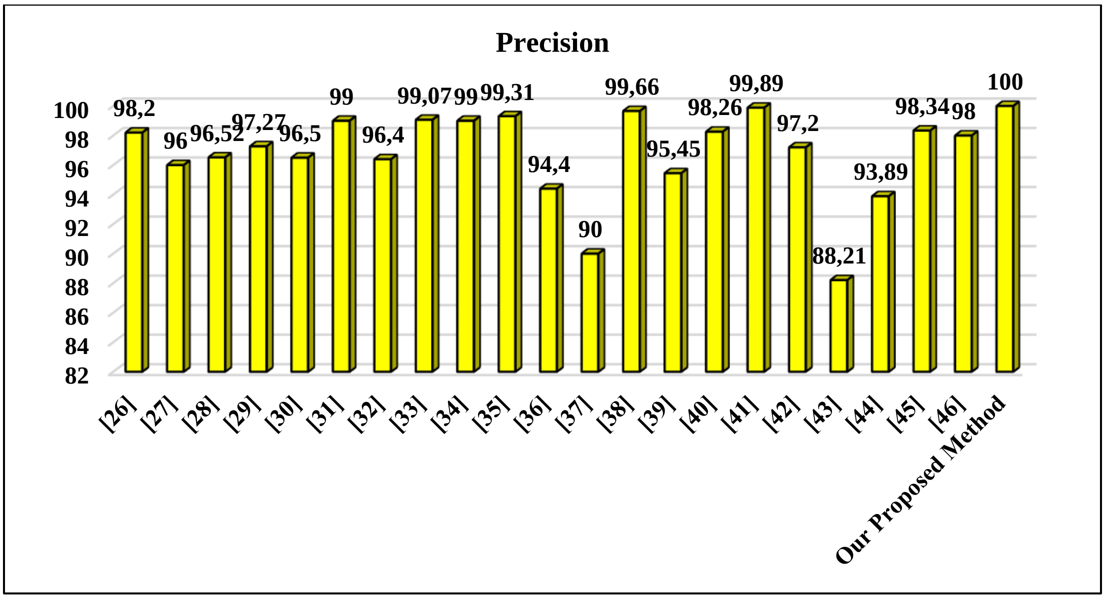

Figure 5. 15. Precision's results comparison.

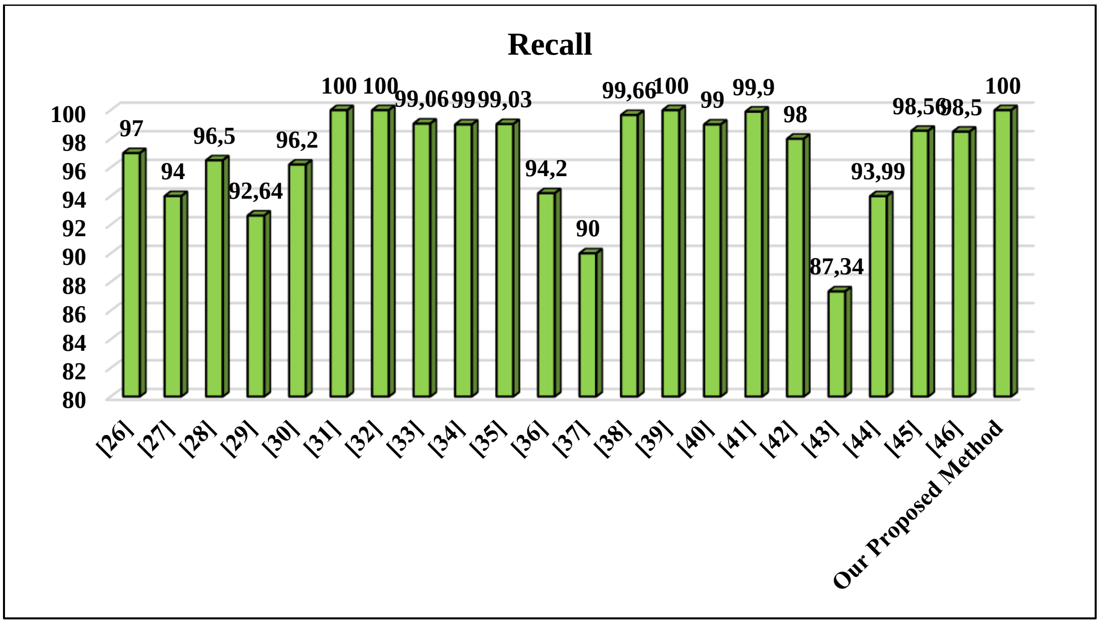

Figure 5. 16. Recall's results comparison.

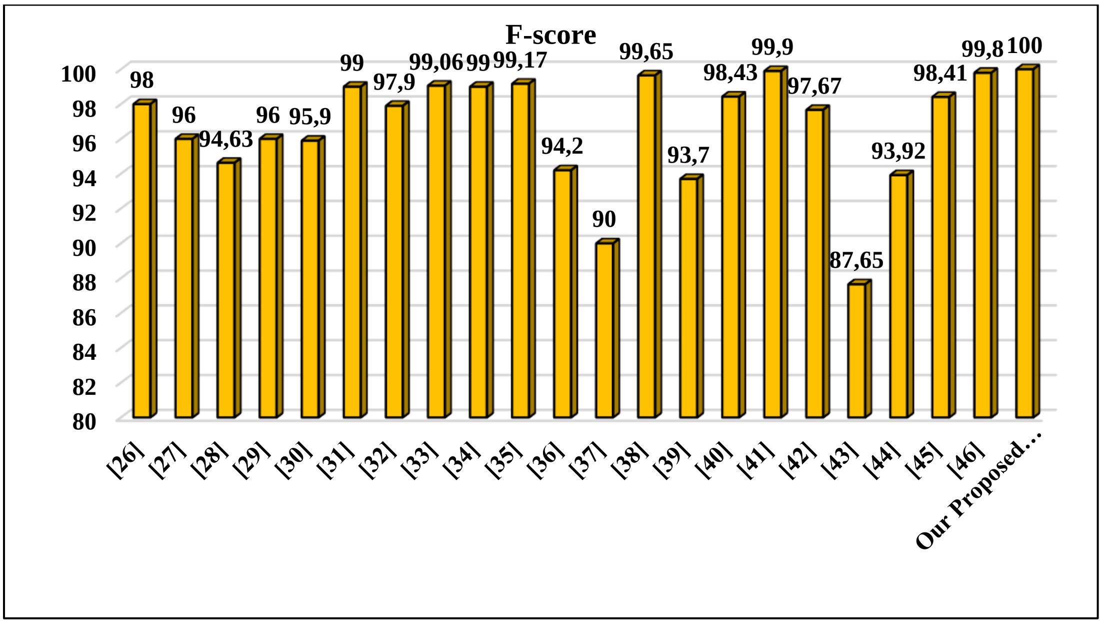

Figure 5. 17. F-score results comparison.

5.3. IMPLEMENTATION OF THE PROPOSED SYSTEM

At first, the main interface of the program is programmed with Java Programming Language as shown in Fig. (5.18) as follows:

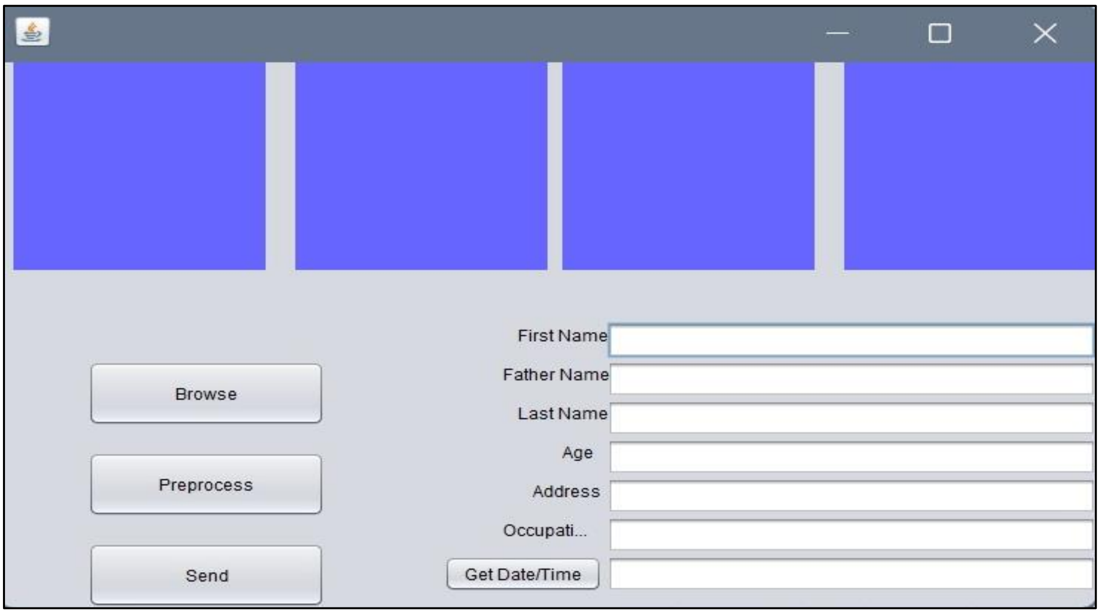

Figure 5. 18. Browsing interface.

Then the patient's information is entered, which is the patient's name, family name, age, and address, as shown in Figure 5.19. After that, an image is selected from the dataset as shown in Figure 5.20, then this image is attached to the patient's information, as shown in Figure 5.21. Followed by the image pre-processing process through grayscale conversion and histogram equalization as shown in Figure 5.22.

Figure 5. 19. Patient's information.

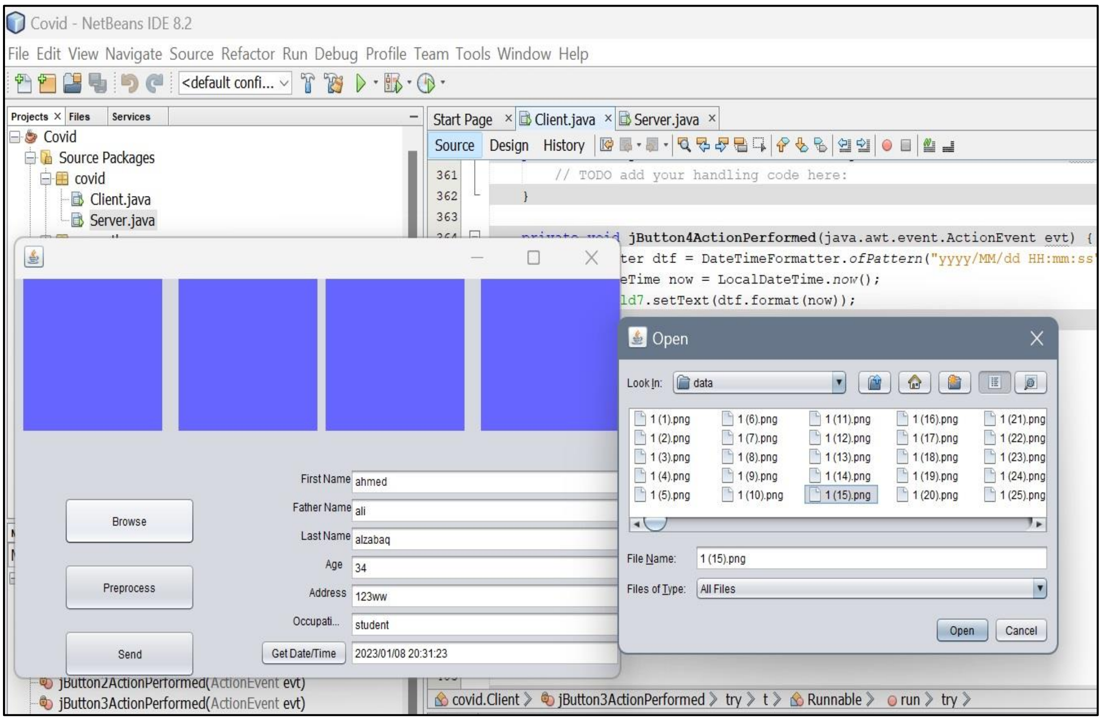

Figure 5. 20. Select an X-ray image from the dataset.

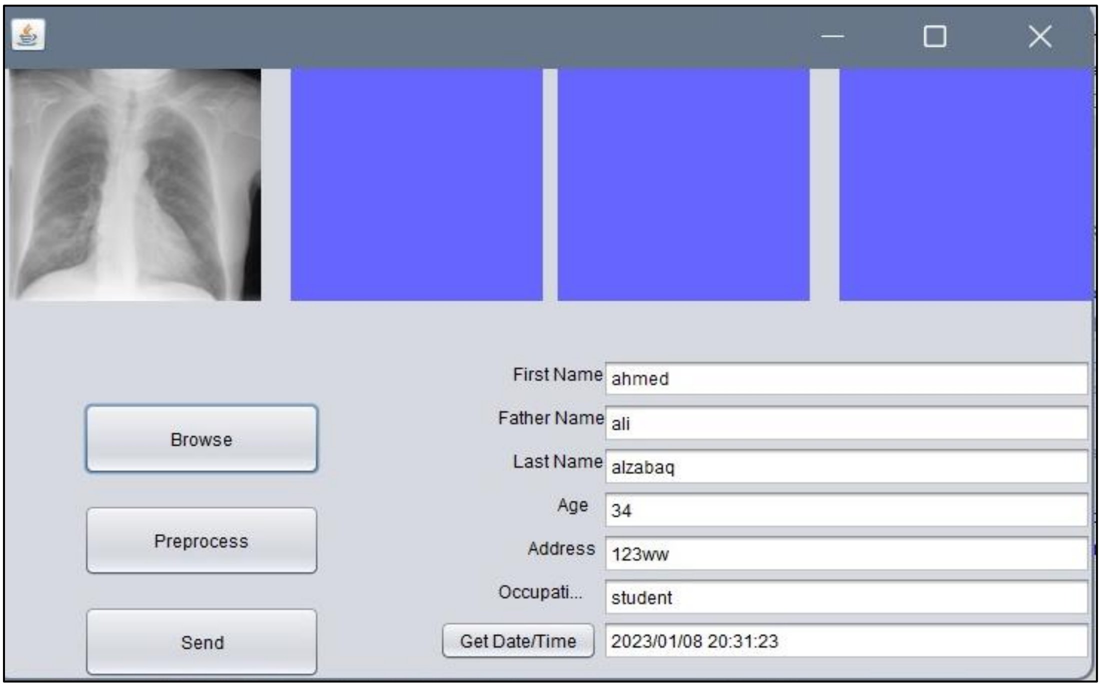

Figure 5. 21. Attach an image of the patient’s information.

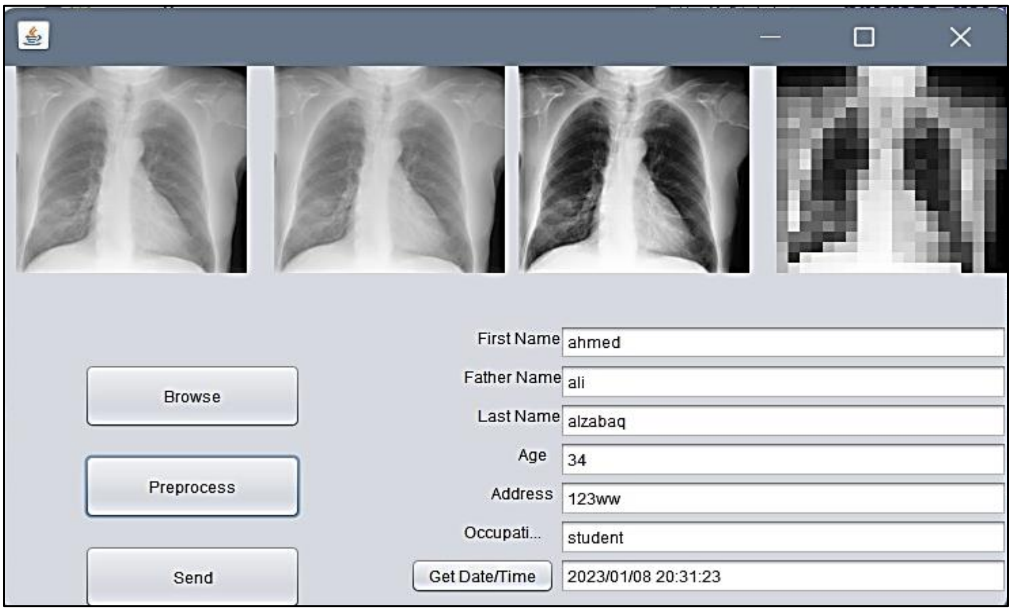

Figure 5. 22. Preprocessing phase of the X-ray image.

The information is sent to the server, and in the event that the information arrives, it confirms that as shown in Figure 5.23, to then determine the pathological condition, whether the person is normal “class 0” Figure 5.24, or infected with Covid-19 “class 1” as shown in Figure 5.25, or has pneumonia “class 2” as shown in Figure 5.26, and finally has a lung opacity “class 3” as shown in Figure 5.27.

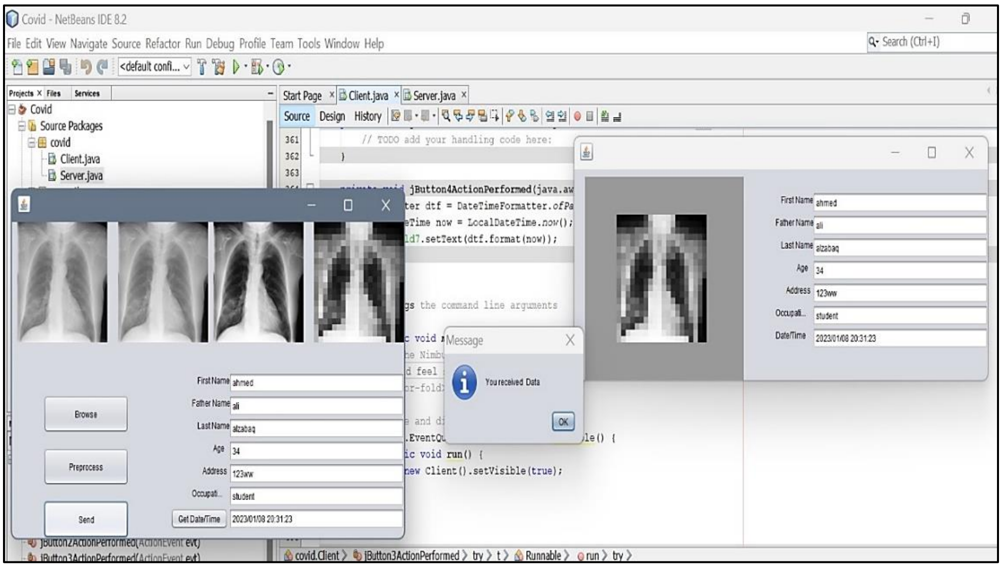

Figure 5. 23. Sending information to the server.

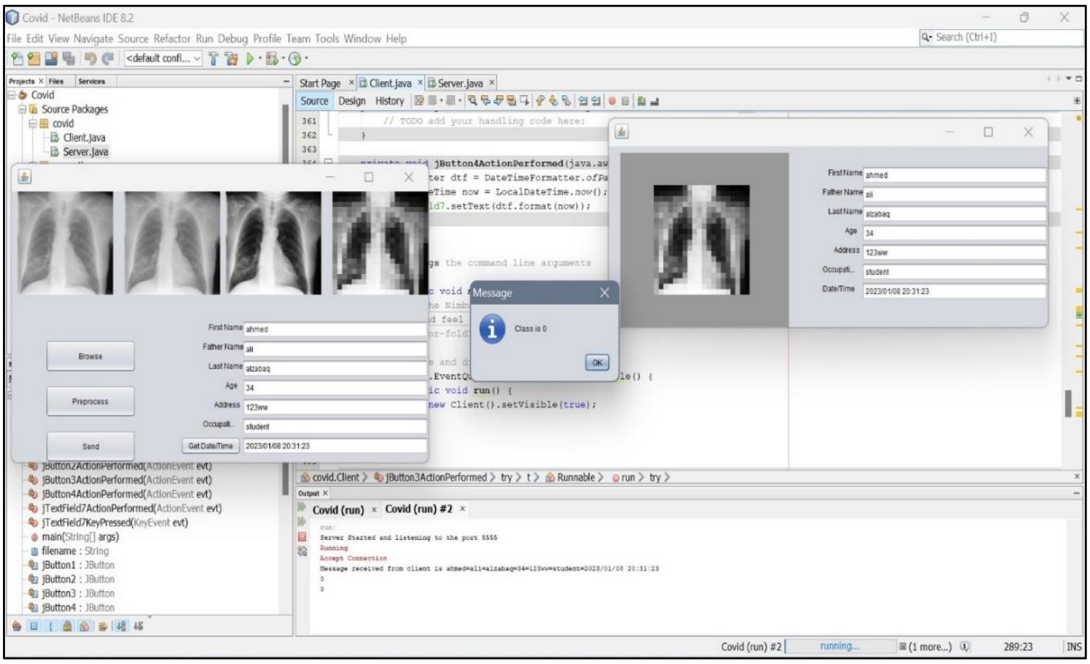

Figure 5. 24. Class zero (normal).

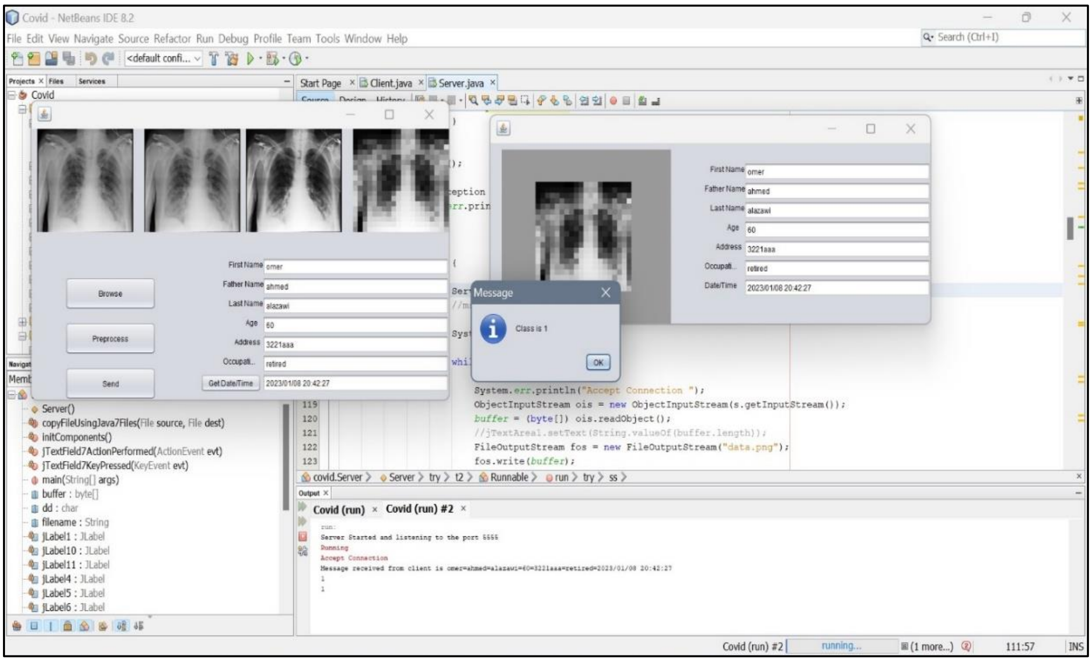

Figure 5. 25. Class one (COVID).

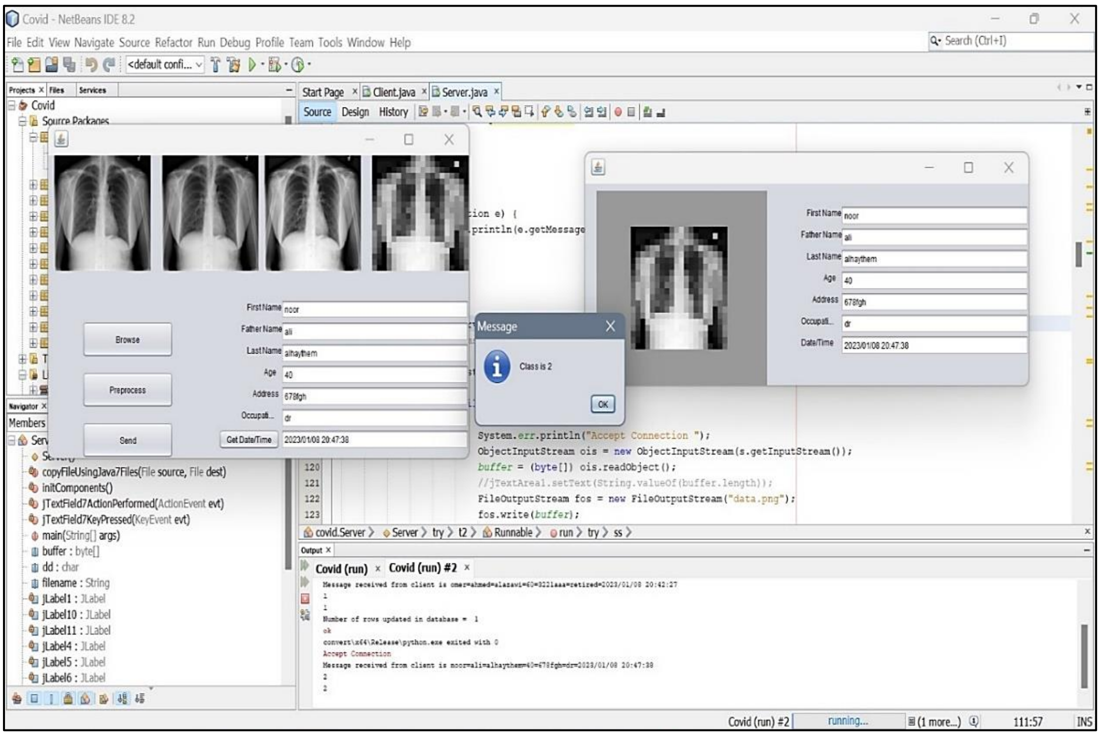

Figure 5. 26. Class two (Viral Pneumonia).

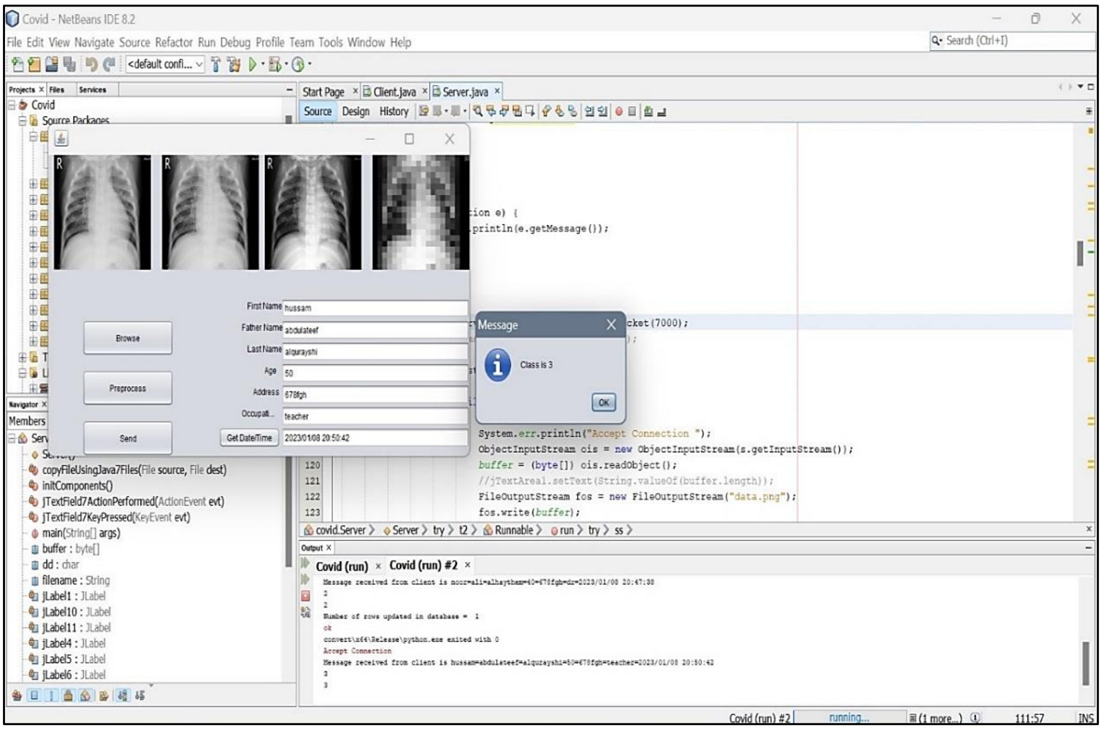

Figure 5. 27. Class three (Lung Opacity).

After that, the data is stored in the database in the Oracle program, as shown in Figure 5.28, with all the information that was entered, in addition to the type of disease that was identified through the X-ray image.

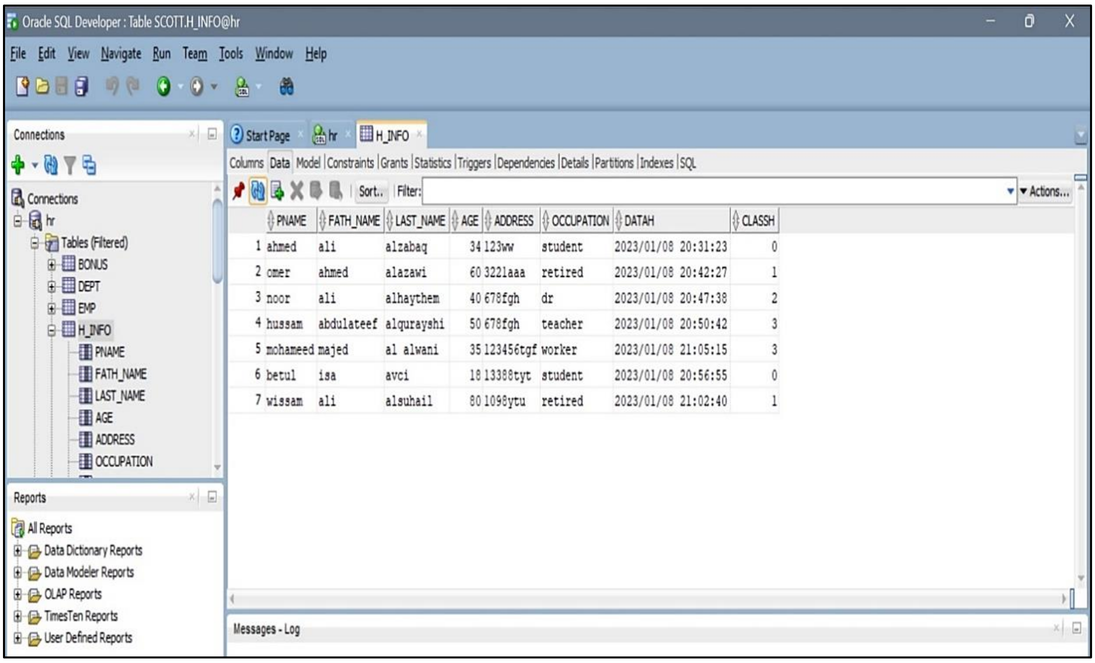

Figure 5. 28. Patient information in the Oracle database.

PART 6

CONCLUSIONS AND RECOMMENDATIONS

The following are the key discoveries made during the creation and implementation of the suggested system, as well as the achievement of its outcomes:

1. The suggested system included a preprocessing stage represented by the grayscale image transformation and histogram equalization processes which were carried out as a crucial stage since it helped to prepare the dataset for the proposed deep learning models. The random sampling approach was adopted; this method provides adjustable propriety in data splitting in both the training and testing phases.
2. Feature reduction approaches being used by LDA and GLCM work to keep essential features that can assist to raise the accuracy of the proposed system while removing features that are regarded unnecessary, which has a significant influence on increasing the accuracy of the suggested system while also lowering execution time.
3. The possibility of the suggested system to classify more than one disease using the Covid-19 Radiography dataset these diseases are (COVID-19, Viral Pneumonia, and Lung Opacity).
4. COVID-19 disease is one of the serious diseases that affect the respiratory system that has occupied the world over the past two years. Therefore, the proposed approach can contribute significantly to the early detection of this disease and contribute to its treatment and limit its spread.
5. CNN-1D used in the suggested models is more dependable, achieving the best results, and it is unaffected by the size or kind of dataset. The attained accuracy was 99.94%

The following issues have been discovered that will need to be resolved in the future to construct the proposed models:

1. Using other types of medical images to classify diseases of the respiratory system, such as (CT Scans, Sputum Smear Microscopy, and Histopathology) images.
2. Classification of other diseases of the respiratory system, which are no less dangerous than the diseases that have been classified, such as lung cancer and asthma.

REFERENCES

1. Rahaman, M. M., Li, C., Yao, Y., Kulwa, F., Rahman, M. A., Wang, Q., Qi, S., Kong, F., Zhu, X., and Zhao, X., "Identification of COVID-19 samples from chest X-Ray images using deep learning: A comparison of transfer learning approaches", ***Journal Of X-Ray Science And Technology***, 28 (5): 821–839 (2020).

2. Shantanam, S. and MUELLER, "HHS Public Access", ***Physiology & Behavior***, 176 (1): 139–148 (2018).

3. Wu, C., Luo, C., Xiong, N., Zhang, W., and Kim, T. H., "A greedy deep learning method for medical disease analysis", ***IEEE Access***, 6: 20021–20030 (2018).

4. Ma, J., Song, Y., Tian, X., Hua, Y., Zhang, R., and Wu, J., "Survey on deep learning for pulmonary medical imaging", ***Frontiers Of Medicine***, 14 (4): 450–469 (2020).

5. Rajaraman, S., Candemir, S., Xue, Z., Alderson, P. O., Kohli, M., Abuya, J., Thoma, G. R., and Antani, S., "A novel stacked generalization of models for improved TB detection in chest radiographs", ***Proceedings Of The Annual International Conference Of The IEEE Engineering In Medicine And Biology Society, EMBS***, 2018-July: 718–721 (2018).

6. Hwa Kieu, S. T., Bade, A., Ahmad Hijazi, M. H., and Kolivand, H., "A survey of deep learning for lung disease detection on medical images: State-of-the-art, taxonomy, issues and future directions", ***Journal Of Imaging***, 6 (12): (2020).

7. Shah, S., Mehta, H., and Sonawane, P., "Pneumonia detection using convolutional neural networks", ***Proceedings Of The 3rd International Conference On Smart Systems And Inventive Technology, ICSSIT 2020***, 9 (04): 933–939 (2020).

8. Szepesi, P. and Szilágyi, L., "Detection of pneumonia using convolutional neural networks and deep learning", ***Biocybernetics And Biomedical Engineering***, 42 (3): 1012–1022 (2022).

9. Jaiswal, A. K., Tiwari, P., Kumar, S., Gupta, D., Khanna, A., and Rodrigues, J. J. P. C., "Identifying pneumonia in chest X-rays: A deep learning approach", ***Measurement: Journal Of The International Measurement Confederation***, 145: 511–518 (2019).

10. Alhudhaif, A., Polat, K., and Karaman, O., "Determination of COVID-19 pneumonia based on generalized convolutional neural network model from chest X-ray images", ***Expert Systems With Applications***, 180 (March): 115141 (2021).

11. Agostini, A., Floridi, C., Borgheresi, A., Badaloni, M., Esposto Pirani, P., Terilli, F., Ottaviani, L., and Giovagnoni, A., "Proposal of a low-dose, long-pitch, dual-source chest CT protocol on third-generation dual-source CT using a tin filter for spectral shaping at 100 kVp for CoronaVirus Disease 2019 (COVID-19) patients: a feasibility study", ***Radiologia Medica***, 125 (4): 365–373 (2020).

12. Cozzi, D., Cavigli, E., Moroni, C., Smorchkova, O., Zantonelli, G., Pradella, S., and Miele, V., "Ground-glass opacity (GGO): a review of the differential diagnosis in the era of COVID-19", ***Japanese Journal Of Radiology***, 39 (8): 721–732 (2021).

13. Akter, S., Shamrat, F. M. J. M., Chakraborty, S., Karim, A., and Azam, S., "Covid-19 detection using deep learning algorithm on chest X-ray images", ***Biology***, 10 (11): (2021).

14. Rothan, H. A. and Byrareddy, S. N., "Epidemiology and Pathogenesis of Coronavirus Disease (COVID-19)", ***Novel Research In Microbiology Journal***, 4 (2): 675–687 (2020).

15. Liu, C., Zhou, Q., Li, Y., Garner, L. V., Watkins, S. P., Carter, L. J., Smoot, J., Gregg, A. C., Daniels, A. D., Jervey, S., and Albaiu, D., "Research and Development on Therapeutic Agents and Vaccines for COVID-19 and Related Human Coronavirus Diseases", ***ACS Central Science***, 6 (3): 315–331 (2020).

16. Grey, "Since January 2020 Elsevier has created a COVID-19 resource centre with free information in English and Mandarin on the novel coronavirus COVID-19 . The COVID-19 resource centre is hosted on Elsevier Connect , the company ' s public news and information.", ***Psychiatry Research***, 14(4) (January): 293 (2020).

17. Kim, G. B., Jung, K. H., Lee, Y., Kim, H. J., Kim, N., Jun, S., Seo, J. B., and Lynch, D. A., "Comparison of Shallow and Deep Learning Methods on Classifying the Regional Pattern of Diffuse Lung Disease", ***Journal Of Digital Imaging***, 31 (4): 415–424 (2018).

18. Shoeibi, A., Khodatars, M., Alizadehsani, R., Ghassemi, N., Jafari, M., Moridian, P., Khadem, A., Sadeghi, D., Hussain, S., Zare, A., Sani, Z. A., Bazeli, J., Khozeimeh, F., Khosravi, A., Nahavandi, S., Acharya, U. R., and Gorriz, J. M., "Automated Detection and Forecasting of COVID-19 using Deep Learning Techniques: A Review", (2020).

19. Khemasuwan, D., Sorensen, J. S., and Colt, H. G., "Artificial intelligence in pulmonary medicine: Computer vision, predictive model and covid-19", ***European Respiratory Review***, 29 (157): 1–16 (2020).

20. Liu, Y. H., "Feature Extraction and Image Recognition with Convolutional Neural Networks", ***Journal Of Physics: Conference Series***, 1087 (6): 0–7 (2018).

21. Costa, Y. M. G., Silva, S. A., Teixeira, L. O., Pereira, R. M., Bertolini, D., Britto, A. S., Oliveira, L. S., and Cavalcanti, G. D. C., "COVID-19 Detection on Chest X-ray and CT Scan: A Review of the Top-100 Most Cited Papers", ***Sensors***, 22

(19): 1–26 (2022).

22. Shafi, I., Din, S., Khan, A., Díez, I. D. L. T., Casanova, R. del J. P., Pifarre, K. T., and Ashraf, I., "An Effective Method for Lung Cancer Diagnosis from CT Scan Using Deep Learning-Based Support Vector Network", ***Cancers***, 14 (21): 5457 (2022).

23. Mithra, K. S. and Sam Emmanuel, W. R., "Automated identification of mycobacterium bacillus from sputum images for tuberculosis diagnosis", ***Signal, Image And Video Processing***, 13 (8): 1585–1592 (2019).

24. Hanley, B., Naresh, K. N., Roufosse, C., Nicholson, A. G., Weir, J., Cooke, G. S., Thursz, M., Manousou, P., Corbett, R., Goldin, R., Al-Sarraj, S., Abdolrasouli, A., Swann, O. C., Baillon, L., Penn, R., Barclay, W. S., Viola, P., and Osborn, M., "Histopathological findings and viral tropism in UK patients with severe fatal COVID-19: a post-mortem study", ***The Lancet Microbe***, 1 (6): e245–e253 (2020).

25. Liu, H., Wang, L., Nan, Y., Jin, F., Wang, Q., and Pu, J., "SDFN: Segmentation-based deep fusion network for thoracic disease classification in chest X-ray images", ***Computerized Medical Imaging And Graphics***, 75: 66–73 (2019).

26. Sharma, S., "COVID-19 prediction from chest X-ray images using deep convolutional neural network", ***Artificial Intelligence And Machine Learning For EDGE Computing***, (March 2020): 315–324 (2022).

27. Hussain, M. G. and Shiren, Y., "Recognition of COVID-19 Disease Utilizing X-Ray Imaging of the Chest Using CNN", ***Proceedings - 2021 International Conference On Computing, Electronics And Communications Engineering, ICCECE 2021***, 71–76 (2021).

28. Tang, Y. X., Tang, Y. B., Peng, Y., Yan, K., Bagheri, M., Redd, B. A., Brandon, C. J., Lu, Z., Han, M., Xiao, J., and Summers, R. M., "Automated abnormality classification of chest radiographs using deep convolutional neural networks", ***Npj Digital Medicine***, 3 (1): (2020).

29. Pandit, M. K., Banday, S. A., Naaz, R., and Chishti, M. A., "Automatic detection of COVID-19 from chest radiographs using deep learning", ***Radiography***, 27 (2): 483–489 (2021).

30. Jadon, S., "COVID-19 detection from scarce chest x-ray image data using few-shot deep learning approach", 1 (2021).

31. Uddin, A., Talukder, B., Monirujjaman Khan, M., and Zaguia, A., "Study on Convolutional Neural Network to Detect COVID-19 from Chest X-Rays", ***Mathematical Problems In Engineering***, 2021: (2021).

32. Mahesh, P., Prathyusha, Y. G., Sahithi, B., and Nagendram, S., "Covid-19 Detection from Chest X-Ray using Convolution Neural Networks", ***Journal Of Physics: Conference Series***, 1804 (1): 0–10 (2021).

33. Yang, D., Martinez, C., Visuña, L., Khandhar, H., Bhatt, C., and Carretero, J., "Detection and analysis of COVID-19 in medical images using deep learning techniques", ***Scientific Reports***, 11 (1): 1–13 (2021).

34. Arias-Garzón, D., Alzate-Grisales, J. A., Orozco-Arias, S., Arteaga-Arteaga, H. B., Bravo-Ortiz, M. A., Mora-Rubio, A., Saborit-Torres, J. M., Serrano, J. Á. M., de la Iglesia Vayá, M., Cardona-Morales, O., and Tabares-Soto, R., "COVID-19 detection in X-ray images using convolutional neural networks", ***Machine Learning With Applications***, 6 (August): 100138 (2021).

35. Hossain, M. B., Iqbal, S. M. H. S., Islam, M. M., Akhtar, M. N., and Sarker, I. H., "Transfer learning with fine-tuned deep CNN ResNet50 model for classifying COVID-19 from chest X-ray images", ***Informatics In Medicine Unlocked***, 30 (March): 100916 (2022).

36. Boulila, W., Ammar, A., Benjdira, B., and Koubaa, A., "Securing the Classification of COVID-19 in Chest X-ray Images: A Privacy-Preserving Deep Learning Approach", ***Proceedings - 2022 2nd International Conference Of Smart Systems And Emerging Technologies, SMARTTECH 2022***, 220–225 (2022).

37. Abdul Gafoor, S., Sampathila, N., Madhushankara, M., and Swathi, K. S., "Deep learning model for detection of COVID-19 utilizing the chest X-ray images", ***Cogent Engineering***, 9 (1): (2022).

38. Asif, S., Zhao, M., Tang, F., and Zhu, Y., "A deep learning-based framework for detecting COVID-19 patients using chest X-rays", ***Multimedia Systems***, 28 (4): 1495–1513 (2022).

39. Sarki, R., Ahmed, K., Wang, H., Zhang, Y., and Wang, K., "Automated detection of COVID-19 through convolutional neural network using chest x-ray images", ***PLoS ONE***, 17 (1 January): 1–26 (2022).

40. Hashmi, M. F., Katiyar, S., Keskar, A. G., Bokde, N. D., and Geem, Z. W., "Efficient pneumonia detection in chest xray images using deep transfer learning", ***Diagnostics***, 10 (6): 1–23 (2020).

41. Karar, M. E., Hemdan, E. E. D., and Shouman, M. A., "Cascaded deep learning classifiers for computer-aided diagnosis of COVID-19 and pneumonia diseases in X-ray scans", ***Complex And Intelligent Systems***, 7 (1): 235–247 (2021).

42. Brunese, L., Mercaldo, F., Reginelli, A., and Santone, A., "Explainable Deep Learning for Pulmonary Disease and Coronavirus COVID-19 Detection from X-rays", ***Computer Methods And Programs In Biomedicine***, 196: 105608 (2020).

43. Apostolopoulos, I. D., Aznaouridis, S. I., and Tzani, M. A., "Extracting Possibly Representative COVID-19 Biomarkers from X-ray Images with Deep Learning Approach and Image Data Related to Pulmonary Diseases", ***Journal Of Medical And Biological Engineering***, 40 (3): 462–469 (2020).

44. Mabrouk, A., Redondo, R. P. D., Dahou, A., Elaziz, M. A., and Kayed, M., "Pneumonia Detection on Chest X-ray Images Using Ensemble of Deep Convolutional Neural Networks", ***Applied Sciences (Switzerland)***, 12 (13): (2022).

45. Ullah, N., Khan, J. A., Almakdi, S., Khan, M. S., Alshehri, M., Alboaneen, D., and Raza, A., "A Novel CovidDetNet Deep Learning Model for Effective COVID-19 Infection Detection Using Chest Radiograph Images", ***Applied Sciences (Switzerland)***, 12 (12): (2022).

46. Abbas, A., Abdelsamea, M. M., and Gaber, M. M., "DeTrac: Transfer Learning of Class Decomposed Medical Images in Convolutional Neural Networks", ***IEEE Access***, 8: 74901–74913 (2020).

47. Latif, S., Usman, M., Manzoor, S., Iqbal, W., Qadir, J., Tyson, G., Castro, I., Razi, A., Kamel Boulos, M. N., Weller, A., and Crowcroft, J., "Leveraging Data Science to Combat COVID-19: A Comprehensive Review", ***IEEE Transactions On Artificial Intelligence***, 1 (1): 85–103 (2020).

48. AYKANAT, M., KILIÇ, Ö., KURT, B., and SARYAL, S. B., "Lung disease classification using machine learning algorithms", ***International Journal Of Applied Mathematics Electronics And Computers***, 8 (4): 125–132 (2020).

49. Dey, N., Zhang, Y. D., Rajinikanth, V., Pugalenthi, R., and Raja, N. S. M., "Customized VGG19 Architecture for Pneumonia Detection in Chest X-Rays", ***Pattern Recognition Letters***, 143: 67–74 (2021).

50. Kido, S., Hirano, Y., and Hashimoto, N., "Detection and classification of lung abnormalities by use of convolutional neural network (CNN) and regions with CNN features (R-CNN)", ***2018 International Workshop On Advanced Image Technology, IWAIT 2018***, 1–4 (2018).

51. Sasikumar, S., Renjith, P. N., Ramesh, K., and Sankaran, K. S., "Attention based recurrent neural network for lung cancer detection", (2020).

52. Hu, H., Li, Q., Zhao, Y., and Zhang, Y., "Parallel Deep Learning Algorithms with Hybrid Attention Mechanism for Image Segmentation of Lung Tumors", ***IEEE Transactions On Industrial Informatics***, 17 (4): 2880–2889 (2021).

53. Souid, A., Sakli, N., and Sakli, H., "Classification and predictions of lung diseases from chest x- rays using mobilenet v2", ***Applied Sciences (Switzerland)***, 11 (6): (2021).

54. Wang, X., Chen, T., Li, D., and Yu, S., "Processing Methods for Digital Image Data Based on the Geographic Information System", ***Complexity***, 2021: (2021).

55. Richards, J. A., "Remote Sensing Digital Image Analysis: An Introduction", Remote Sensing Digital Image Analysis: An Introduction, 1–494 (2013).

56. Tyagi, V., "Understanding Digital Image Processing A SCIENCE PUBLISHERS BOOK", .

57. Mohan, V. M., Kanaka Durga, R., Devathi, S., and Srujan Raju, K., "Image processing representation using binary image; grayscale, color image, and histogram", (2016).

58. Karimi, A.-H. K., Chung, A. G., Shafiee, M. J., Khalvati, F., Haider, M. A., Ghodsi, A., and Wong, A., "Image Analysis and Recognition", (2016).

59. Li, P., Wang, H., Yu, M., and Li, Y., "Overview of Image Smoothing Algorithms", (2021).

60. Chen, T., "AN ADAPTIVE IMAGE SHARPENING SCHEME", (July 2019): (2020).

61. Buckner, C. A., Lafrenie, R. M., Dénommée, J. A., Caswell, J. M., and Want, D. A., "Complementary and alternative medicine use in patients before and after a cancer diagnosis", ***Current Oncology***, 25 (4): e275–e281 (2018).

62. Mohapatra, B. N., "Image edge detection techniques", 5 (15): 15–19 (2019).
63. Shi, P., Duan, M., Yang, L., Feng, W., and Ding, L., "An Improved U-Net Image Segmentation Method and Its", 1–17 (2022).

64. Husni, A., Shapri, M., and Abdullah, M. Z., "Accurate retrieval of region of interest for estimating point spread function and image deblurring", ***The Imaging Science Journal***, 00 (0): 1–22 (2017).

65. Danon, D., "Image resizing by reconstruction from deep features", 7 (4): 453–466 (2021).

66. Bekhet, S., Hassaballah, M., Kenk, M. A., and Hameed, M. A., "An Artificial Intelligence Based Technique for COVID-19 Diagnosis from Chest X-Ray", (2020).

67. Chawla, P., "Diabetes India Conference (2022) and Journal, “Diabetes and Metabolic Syndrome: Clinical Research and Reviews”: A Tribute to Dr Shaukat Sadikot", ***Diabetes And Metabolic Syndrome: Clinical Research And Reviews***, 16 (7): 102557 (2022).

68. Ricciardi, C., Valente, A. S., Edmunds, K., and Santini, S., "Linear discriminant analysis and principal component analysis to predict coronary artery disease", (2020).

69. Al-Abaji, M. A. and Salih, M. M., "The Using of PCA, Wavelet and GLCM In Face Recognition System, A Comparative Study", ***JOURNAL OF UNIVERSITY OF BABYLON For Pure And Applied Sciences***, 26 (10): 131–139 (2018).

70. Promotionsausschuss, V. and Baltruschat, I. M., "Deep Learning for Automatic

Lung Disease Analysis in Chest X-rays", (2021).

71. Fourati, F. and Alouini, M.-S., "Artificial intelligence for satellite communication: A review", ***Intelligent And Converged Networks***, 2 (3): 213–243 (2021).

72. Sah, S., "Machine Learning: A Review of Learning Types", ***ResearchGate***, (July): (2020).

73. Berrar, D., "Cross-validation", ***Encyclopedia Of Bioinformatics And Computational Biology: ABC Of Bioinformatics***, 1–3 (January 2018): 542–545 (2018).

74. Yuan, Z., Lu, Y., Wang, Z., and Xue, Y., "Droid-Sec: Deep learning in android malware detection", ***Computer Communication Review***, 44 (4): 371–372 (2015).

75. Aouedi, O., Piamrat, K., and Parrein, B., "Intelligent Traffic Management in Next-Generation Networks", ***Future Internet***, 14 (2): (2022).

76. El-Yaniv, R. and Souroujon, O., "Iterative double clustering for unsupervised and semi-supervised learning", ***Lecture Notes In Computer Science (Including Subseries Lecture Notes In Artificial Intelligence And Lecture Notes In Bioinformatics)***, 2167: 121–132 (2001).

77. Omar, F., Nasim, Z., and Izharuddin, M., "Multi-classification of COVID-19 and pneumonia in chest X-ray images using convolutional neural network", ***Proceedings Of The 1st International Conference On Advances In Computing And Future Communication Technologies, ICACFCT 2021***, 248–252 (2021).

78. Kang, X., Song, B., and Sun, F., "A deep similarity metric method based on incomplete data for traffic anomaly detection in IoT", ***Applied Sciences (Switzerland)***, 9 (1): (2019).

79. Dhiman, R., Joshi, G., and Rama Krishna, C., "A deep learning approach for Indian sign language gestures classification with different backgrounds", ***Journal Of Physics: Conference Series***, 1950 (1): (2021).

80. Veithzal Rivai, D., Thesis, M., Sloane, G. M. T., Pröbstl-Haider, U., Rogers, A. W., Paciarotti, C., Cesaroni, A., Gorlova, N. I., Troska, Z. A., Starovojtova, L. I., Demidova, T. E., Akhtyan, A. G., Shcheglova, A. S., Dunne, J. P., Smith, R. P., Westerdal, M., Rights, A., Copyright, I., Cuskelly, G., Fredline, L., Kim, E., Barry, S., Kappelides, P., Bíl, M., Heigl, F., Janoška, Z., Vercayie, D., and Perkins, S. E., "Title", ***Kaos GL Dergisi***, 8 (75): 147–154 (2020).

81. Bai, Y., "RELU-Function and Derived Function Review", ***SHS Web Of Conferences***, 144: 02006 (2022).

82. Chakraborty, P. and Tharini, C., "Pneumonia and Eye Disease Detection using Convolutional Neural Networks", ***Engineering, Technology & Applied Science Research***, 10 (3): 5769–5774 (2020).

83. Helen Josephine, V. L., Nirmala, A. P., and Alluri, V. L., "Impact of Hidden Dense Layers in Convolutional Neural Network to enhance Performance of Classification Model", ***IOP Conference Series: Materials Science And Engineering***, 1131 (1): 012007 (2021).

84. Pelletier, C., Webb, G. I., and Petitjean, F., "Temporal convolutional neural network for the classification of satellite image time series", ***Remote Sensing***, 11 (5): 1–25 (2019).

85. Kiranyaz, S., Avci, O., Abdeljaber, O., Ince, T., Gabbouj, M., and Inman, D. J., "1D convolutional neural networks and applications: A survey", ***Mechanical Systems And Signal Processing***, 151: 107398 (2021).

86. Markoulidakis, I., Kopsiaftis, G., Rallis, I., and Georgoulas, I., "Multi-Class Confusion Matrix Reduction method and its application on Net Promoter Score classification problem", ***ACM International Conference Proceeding Series***, 412–419 (2021).

RESUME

AHMED ABDULATEEF ALZABAQ graduated from elementary education in Baghdad-Iraq at (AL-Qastal school). He completed his high school education at (Adhamiya high school) in Baghdad-Iraq also, then he obtained a bachelor’s degree from Al-Rafidain University College of Computer Techniques Engineering in 2013. After graduation, he worked in many companies in Iraq in his position as (Sales Representative, and IT manager...) after he moved to UAE and he worked IT manager for 2 years. To complete his M.Sc. education, he moved to Karabuk/Turkey in 2020. He started his master’s education at the department of computer engineering at Karabuk University.